26717

NAME OF AUTHOR *NOM DE L'AUTEUR* Robert Leslie Brooks

TITLE OF THESIS *TITRE DE LA THÈSE* Quantum Beats in Beam-foil Spectroscopy.

UNIVERSITY *UNIVERSITÉ* University of Alberta

DEGREE FOR WHICH THESIS WAS PRESENTED
GRADE POUR LEQUEL CETTE THÈSE FUT PRÉSENTÉE Master of Science

YEAR THIS DEGREE CONFERRED *ANNÉE D'OBTENTION DE CE GRADE* 1975

NAME OF SUPERVISOR *NOM DU DIRECTEUR DE THÈSE* Dr. Eric H. Pinnington

DATED *DATE* Aug 18, 75   SIGNED/*SIGNÉ* Robert L. Brooks

PERMANENT ADDRESS/*RÉSIDENCE FIXE* 2037 Oakmont St.

Philadelphia, Pa. 19152

NL-91 (3-74)

THE UNIVERSITY OF ALBERTA

QUANTUM BEATS IN BEAM-FOIL SPECTROSCOPY

by

ROBERT LESLIE BROOKS

A THESIS

SUBMITTED TO THE FACULTY OF GRADUATE STUDIES AND RESEARCH

IN PARTIAL FULFILLMENT OF THE REQUIREMENTS FOR THE DEGREE

OF MASTER OF SCIENCE

DEPARTMENT OF PHYSICS

EDMONTON, ALBERTA

FALL, 1975

THE UNIVERSITY OF ALBERTA

FACULTY OF GRADUATE STUDIES AND RESEARCH

The undersigned certify that they have read, and
recommend to the Faculty of Graduate Studies and
Research, for acceptance, a thesis entitled QUANTUM
BEATS IN BEAM-FOIL SPECTROSCOPY submitted by Robert
Leslie Brooks in partial fulfillment of the require-
ments for the degree of Master of Science.

....
Supervisor

....

....

....

DATE: July 7 1975

TO MY PARENTS

iv

ABSTRACT

A review of quantum beats in beam-foil spectro-
scopy is presented. Coherence and alignment conditions
are defined and discussed with respect to the obser-
vation of zero-field, Zeeman and Stark beats. The
experimental equipment required to perform quantum-
beat observation is described. Methods of data analysis,
particularly the finite, discrete Fourier transform and
direct least-squares approach, are developed from their
fundamentals and applied to both synthesized and actual
data.

Experiments were performed to observe zero-field
beats in boron III at 2066 Å and Stark beats in boron
V at 749 Å. Electric field calibration was carried
out by the observation of Stark beats in hydrogen
Lyman-α. No quantum beats were conclusively observed
in either boron experiment.

FOREWORD

Beam-foil Spectroscopy at the University of
Alberta was begun in 1967 by Dr. E.H. Pinnington.
Improvements to both the equipment and data analysis
occurred steadily through 1973 from the efforts of
staff members, a former Post Doctoral Fellow, Dr.
D.J.G. Irwin, and former students, Drs. C.C. Lin and
A.E. Livingston. These improvements included purchase
of a new vacuum ultraviolet spectrometer and photon-
counting detectors, design and manufacture of several
target chambers, laser alignment of the equipment,
automatic remote data acquisition and development of
an extensive data analysis program for lifetime measure-
ments.

The author joined the group in 1973 and parti-
cipated in his first experiment in Spring 1974. The
purpose of the experiment was the first attempt at the
University of Alberta to observe quantum beats. We were
fortunate to be joined by Dr. H.G. Berry of the
University of Chicago and Argonne National Laboratory
(U.S.) who suggested, during the course of the experi-
ment, the specific attempt to observe Stark beats in
boron V. The attempt was unsuccessful and Dr. Berry
invited Dr. Pinnington and myself to Argonne National
Laboratory in December 1974 to try again with higher
beam energy. Again we failed to observe quantum beats

in boron but did observe them in hydrogen under special experimental conditions which had only recently been reported in the literature.

ACKNOWLEDGEMENTS

TABLE OF CONTENTS

LIST OF TABLES

x

LIST OF FIGURES

CHAPTER I

INTRODUCTION

Beam-foil spectroscopy (BFS) is the study of radiation emitted by a beam of fast moving ions after undergoing excitation by passing through a thin target foil. Pioneered by Stanley Bashkin (Ba 64) at the University of Arizona, interest soon spread to other institutions, particularly following the first international conference on BFS in 1967. Since then, two other international conferences have been held and a fourth is scheduled for September 1975. The proceedings[1] from these conferences offer an excellent review of a new experimental technique in contemporary physics.

The beam-foil light source is characterized by greater advantages and fewer drawbacks than conventional spectroscopic sources. The thin foil, typically 3-15 $\mu g/cm^2$ ($\sim$500 Å) of carbon, gives a sharply defined spatial origin such that distance "downstream" from the foil corresponds to time since excitation. The low particle density eliminates imprisonment of resonance radiation, recombination of ions and electrons, and stimulated emission. The foil excitation easily produces multiply-ionized species in virtually all excited

---

[1] Ba 68, MBB 70, Ba 73.

states. Magnetic mass resolution effectively isolates
the ion of interest thereby eliminating impurities
except in cases such as $^{28}Si^+$ which can be contaminated
with N_2^+ and CO^+ (typical high vacuum residual molecules).
The plethora of spectral lines which are usually.
observed does present a problem with line blending.
The excitation of even the highest energy levels
causes cascading to the level of interest which has·
proven to be the most troublesome drawback.

One obvious application of such a light source
is the measurement of atomic mean lives. Light from
a short segment of the beam ($\sim$0.3-2.0 mm) is first
viewed as close to the foil as geometry allows. Pho-
tons are counted for a preset length of time[2] and then,
the foil is moved a calibrated short distance and the
measurement repeated. By successively moving down the
beam the measured intensity has a characteristic expon-
ential decay whose decay constant yields the mean life.
Were it not for cascades and blends, mean lives could
be as reliably measured as calibration of the beam
velocity permitted. Nevertheless sophisticated computer
routines and diligent analysis by the experimenter are

---

[2] Actually integrated beam current in a Faraday cup,
or light normalization is preferable to time. See
Chapter III.

able to provide lifetime values for almost any element
in several stages of ionization. In many instances
these measurements can be converted into oscillator
strengths which are useful guides for theoretical
atomic structure calculations, especially for heavier
elements. Another recent application is to astro-
physics in which oscillator strengths are needed to
derive element abundances in stars. The need even
extends to rare earth elements whose spectral lines
appear to a remarkable extent in photographic plates
of chemically anomalous stars. Such stars are not rare
but make up nearly 25% of the main sequence including
some of the brightest stars in the sky.

The observation of light modulations along the
beam, or quantum beats (Chapter II), established a
different family of measurements that could be made
with the beam-foil source. These include fine- and
hyperfine-structure measurements, Landé g-values and
Lamb shifts. In addition to such frequency-related
parameters, quantum beat amplitudes and phases may be
related to the degree of non-isotropic excitation of
the atom by the foil, allowing measurements of initial
alignment and orientation.

The initial plan for the present experiment was
to observe the spectrum of boron in the visible and
near ultraviolet, choose a selection of spectral lines

which showed a single, gentle exponential decay and look for zero-field quantum beats between hyperfine levels since that has yet to be observed in boron. However, the failure of peripheral equipment forced us to convert to vacuum ultraviolet spectroscopy and mean-life measurements while the equipment was being repaired. We looked for zero-field beats in the 2066 Å radiation of boron III as this line had looked promising in a previous experiment by Dr. Berry. No beats were observed. A faint line of boron V at 749 Å had also been detected and, being a hydrogenic emission, a Stark-effect quantum beat measurement could have yielded the Lamb shift as discussed in section 2.6. This had not previously been measured and as time limitation[3] prevented us from following our original plan, we concentrated on measuring Stark beats in the B V line.

In the months that followed we attributed failure to observe beats to a poor signal to noise ratio. This experiment was tried again at Argonne in December 1974 where higher beam energy allowed us to collect statistically good data. In fact, although the statistics in the second experiment were adequate, our analysis

---

[3] Accelerator time is allocated by the Radiation Research Committee.

techniques were sufficiently refined for us to know within one week of our return that the boron V data still showed no beats. Reasons for the failure of this Lamb shift measurement will be discussed in Chapter V. As explained in section 2.6 the electric field calibration was performed by examining quantum beats in hydrogen Ly-α. This offered the opportunity to observe "Eck beats", which had been first observed less than one year previously.

Chapter II discusses all of the quantum beat topics mentioned in this introduction. It is presented as a general review and does not employ the mathematical formalism required for a thorough treatment of the phenomena. For example, the use of the irreducible tensor operators and the n-j symbols for angular momenta coupling have been avoided. The chapter does, however, provide a framework within which the varied aspects of quantum beats may be understood and a good starting point for future, more detailed theoretical investigations of this complex subject.

Chapter III is a brief description of the experimental equipment used for this project. Chapter IV describes the methods developed to analyze the data and represents perhaps 80% of all the time spent on this project. As is indicated in

the text, these methods need to be extended before they are generally applicable. However, they were quite adequate for the analysis of data taken for this project. Chapter V is a presentation of the results of these experiments and a discussion of the failures encountered along the way. Criteria for the successful observation of quantum beats in future experiments will be established.

CHAPTER II

REVIEW OF QUANTUM BEATS

Quantum beats are modulations of the radiation emitted from an atom after it has been excited to a coherent superposition of upper levels. The term "quantum beats" seems to have been applied to this phenomenon when first observed by Aleksandrov (Al 63) in radiation emitted by cadmium. Following the theory of Breit (Br 33), Aleksandrov realized that the bandwidth of the 3261 Å radiation from Cd $5s\ ^1S_0 - 5p\ ^3P_1$ was broad enough to encompass the Zeeman splitting of the upper $^3P_1$ term. Consequently he irradiated a gas sample of cadmium placed in a magnetic field with light from a cadmium vapor lamp and observed quantum beats in the radiation from the sample.

The beam-foil light source is ideal for the observation of coherently excited states. From the uncertainty principle ΔE equals $\hbar/\Delta t$ where Δt for beam-foil is the time the atom spends in the foil, typically 10^{-14} sec. This gives a coherence width of about .06 eV (~ 500 cm^{-1} or $\sim 15,000$ GHz), which is 1,000 times greater than the spatial resolution at typical beam velocities. Coherence, then, is guaranteed by the nature of the excitation for all quantum beat experiments performed so far. Further requirements for the

7

·observation of quantum beats will be discussed in section 2.3.

The first beam-foil quantum beat experiment was performed by Bashkin, Bickel and Fink (BBFW 65) who oriented the entrance slit of their spectrometer to view lengthwise along the beam. They observed "bright spots" on the photographic plate when looking at hydrogen Lyman radiation for $n = 3$ to 7., These beats were observed in a very weak magnetic field of 8 gauss and the authors attributed the beats to a motional electric field producing Stark splitting of the excited levels.

Beam-foil experiments rapidly became more sophisticated with the introduction of photon counting techniques and computer analysis of data. Since virtually all experiments centered on obtaining lifetime data it is interesting to note that the first theoretical treatment of quantum beats appeared in Macek's paper, "Theory of Atomic Lifetime Measurements" (Ma 70) in which the author pursued the necessary conditions for quantum beats in order to determine how not to observe them. Quantum beats were considered a source of error for lifetime measurements! But Macek recognized the interesting consequences of his work which predicted the possibility of zero-field beats

(section 2.4) and so published a letter to that effect (Ma 69) prior to his paper on lifetime measurements. Andrä's experiment (An 70) confirmed Macek's prediction and represented the start of detailed,experiments into the quantum beat phenomenon.

This chapter will attempt to give a basic understanding of such experiments and motivate their inauguration at the University of Alberta. The first section describes the coherence condition and derives quantum beats between a simple two-level system. The third section treats the necessary conditions for quantum beat observation using the density matrix formalism which is briefly reviewed in section 2.2. The last three sections treat zero-field beats, Zeeman beats and Stark beats respectively, the latter representing the type of experiment performed for this project.

2.1 Coherence Condition
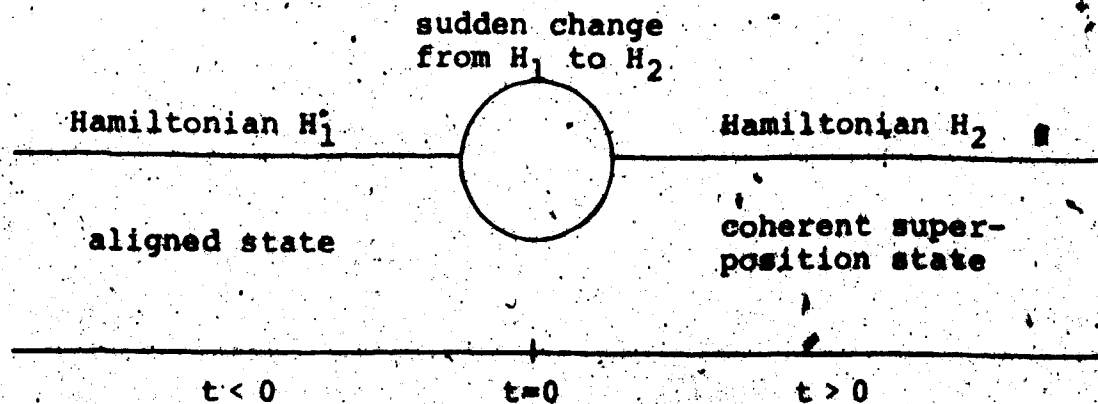
Fig. 1. Evolution of the Hamiltonian

Basically, the quantum mechanical description of quantum beats invokes the sudden perturbation approximation in which the excited atom or ion is considered to be in stationary states of a Hamiltonian H_1 from which it suddenly enters a physical region described by the Hamiltonian H_2. In the description of this latter Hamiltonian the system is no longer in a stationary state but rather a coherent superposition of states whose time evolution gives rise to the beating phenomenon. All quantum beat experiments following foil excitation can be classified into three types according to the Hamiltonians H_1 and H_2 used to describe the system (An 74). These are:

(1) H_1 describes free atoms and H_2 includes external applied fields.

(2) H_1 describes atoms as they leave the foil and H_2 includes external applied fields.

(3) H_1 describes atoms as they leave the foil and H_2 describes free atoms.

Type (1) is applicable to systems in which the external field region is some distance from the foil so that the foil excited atom has decayed to a stationary, excited (perhaps metastable) state from which it radiates after entering the field region. Types (2) and (3) are most commonly used to describe quantum beat experiments in which the field region

(type (2)) begins at the foil. These are called Zeeman beats for magnetic fields, Stark beats for electric fields, and appropriately zero-field beats for no external field.

The simplest quantum mechanical description of a system which predicts an oscillatory modulation of light intensity superposed on an exponential decay is afforded by type (1). A hydrogen atom is prepared in the $|2s\rangle$ state and suddenly enters an electric field. Following Andrä (An 74) the wave equations without electric field can be written:

$$|\psi_{2s}(t)\rangle = |2s\rangle \exp[-(\gamma_s/2 + i\omega_s)t]$$

$$|\psi_{2p}(t)\rangle = |2p\rangle \exp[-(\gamma_p/2 + i\omega_p)t]$$

with $|2s\rangle$ and $|2p\rangle$ solutions of the time independent Schroedinger equation and the time evolution factor including a phenomonological damping term appears in the exponential. In like fashion the solutions in the field region are denoted with primes:

$$|\psi_{2s'}(t)\rangle = |2s'\rangle \exp[-(\gamma_{s'}/2 + i\omega_{s'})t]$$

$$|\psi_{2p'}(t)\rangle = |2p'\rangle \exp[-(\gamma_{p'}/2 + i\omega_{p'})t]$$

The time independent solutions can be expanded according to:

$$|2s'> = a_{ss}|2s> + a_{ps}|2p>$$

$$(2.1)$$

$$|2p'> = a_{sp}|2s> + a_{pp}|2p> \ .$$

Assuming orthonormality of the field-free states, the expansion coefficients are immediately seen to be

$$a_{ss} = <2s|2s'> \qquad a_{ps} = <2p|2s'>$$

$$a_{sp} = <2s|2p'> \qquad a_{pp} = <2p|2p'> \ .$$

Since originally the system was prepared in the $|2s>$ state, at time $t = 0$ the wavefunction must be given by

$$|2s> = |2s'><2s'|2s> + |2p'><2p'|2s> \ .$$

At later times the wavefunction is .

$$|\psi(t)> = a_{ss}^{*}|2s'>\exp[-(\gamma_{s'}/2 + i\omega_{s'})t]$$

$$+ a_{sp}^{*}|2p'>\exp[-(\gamma_{p'}/2 + i\omega_{p'})t] \ .$$

If (2.1) is inserted for the kets on the right this becomes

$$|\psi(t)> = (a_{ss}^{*}a_{ss}|2s> + a_{ss}^{*}a_{ps}|2p>)\exp[-(\gamma_{s'}/2 + i\omega_{s'})t]$$

$$+ (a_{sp}^{*}a_{sp}|2s> + a_{sp}^{*}a_{pp}|2p>)\exp[-(\gamma_{p'}/2 + i\omega_{p'})t] \ .$$

The reason for expressing the wave function in this manner becomes apparent from the expression for the intensity of spontaneous emission:

$$I(t) = \text{Const} \left| <1s | \text{dipole operator} | \psi(t)> \right|^2 \quad .$$

From this it can be seen that transitions can occur only through the $|2p>$ admixture. Finally this yields

$$I(t) = A \exp(-\gamma_{s'} t) + B \exp(-\gamma_{p'} t)$$

$$+ C \exp[-(\gamma_{s'}/2 + \gamma_{p'}/2)t] \cos(\omega_{s'} - \omega_{p'})t \quad .$$

which shows a modulation whose frequency yields the separation of the $|2s'>$, $|2p'>$ levels. If the electric field were calibrated and measurements were made at several field values, an extrapolation to zero field would yield a measurement of the Lamb shift (section 2.6).

The basic concept of quantum beats is that a sudden change of basis allows the observation of a sinusoidal time evolution of the quantum states. The above discussion exemplifies this but is too cumbersome for the treatment of more complex systems. Before tackling the problem with greater generality a brief review of the density matrix will be given.

2.2 Density Matrix

Perhaps the most thorough description of the density matrix was given by Fano (Fa 57) in the Reviews of Modern Physics. Some of the fundamental aspects will be given here following his review.

Consider a state vector ψ whose eigenfunction expansion is

$$\psi = \sum_n c_n u_n$$

with the u_n orthonormal. The mean value of any operator Q is given by

$$\langle Q \rangle = \sum_{n'n} Q_{n'n} c_{n'}^* c_n \ .$$

If a nonpure state is represented by an incoherent super-position of pure states, $\psi^{(i)}$, to each pure state corresponds a mean value $\langle Q \rangle_i$, each with statistical weight $p^{(i)}$, and the mean value of Q for the incoherent super-position is given by the grand average

$$\langle Q \rangle = \sum_i p^{(i)} \langle Q \rangle_i = \sum_{nn'} Q_{n'n} \sum_i p^{(i)} c_{n'}^{(i)*} c_n^{(i)} \ .$$

If one relates the second term to the density matrix then

$$\rho_{nn'} = \sum_i p^{(i)} c_{n'}^{(i)*} c_n^{(i)}$$

and

$$\langle Q \rangle = \sum_{n'n} Q_{n'n} \rho_{nn'} = \sum_{n'} (Q\rho)_{n'n'}$$

or

$$\langle Q \rangle = \mathrm{Tr}(Q\rho) \qquad\qquad (2.2)$$

where Tr indicates the trace of the matrix. Equation (2.2) is taken as the definition of ρ.

Several useful properties follow from the above discussion:

(1) $\rho_{n'n} = \rho_{nn'}^{*}$; the density matrix is Hermitian

(2) $Tr(\rho) = 1$

(3) $\rho_{kk} \geq 0$ in any representation

(4) $Tr(\rho^2) \leq 1$

(5) For pure states $(\rho^2)_{mn} = \rho_{mn}$

Time evolution is given by

$$\frac{\partial \rho}{\partial t} = \frac{-i}{\hbar} [H, \rho]$$

$$\rho(t) = e^{-iHt/\hbar} \rho(0) e^{iHt/\hbar}$$

$$\langle Q \rangle_t = Tr[Q\rho(t)] = Tr[Q(t)\rho(0)] .$$

2.3 Alignment Condition

The intensity of light emitted in the transition from a number of upper states, denoted i, to a number of lower states, f, is given by (FM 73)[1]

$$I(t) = C \sum_{f,i} |\langle f|\underline{e}^* \cdot \underline{D}|i(t)\rangle|^2 \qquad (2.3)$$

with $\underline{e}$ the unit real or complex polarization vector, $\underline{D}$

---

[1] This is a common but not simple result and many older texts offer no derivation whatever; see Mi 70, Chap. 4 and Lo 73, Chap. 8.

the operator (usually dipole) inducing transitions and C is a proportionality factor including those terms needed to make I an energy flux. It could, for example, include an integration over $\underset{\sim}{e}$ if unpolarized light were being observed. Inherent in (2.3) are the assumptions that any splittings within the upper or lower states are small compared to the gross structure involved in the transitions, and that all included transitions fall well within the bandwidth of the detection system (AD 73). If (2.3) is expanded in an eigenbasis of the Hamiltonian H_2 of section 2.1 it becomes

$$I(t) = C \sum_{\substack{f,i \\ \alpha,\beta}} \langle f|\underset{\sim}{e}^*\cdot\underset{\sim}{D}|\alpha\rangle\langle\alpha|\underline{i}(t)\rangle\langle i(t)|\beta\rangle\langle\beta|\underset{\sim}{e}\cdot\underset{\sim}{D}|f\rangle. \qquad (2.4)$$

If $\sum_i |i(t)\rangle\langle i(t)|$ is recognized as the initial density matrix, $\rho(t)$, and $\sum_f |f\rangle\langle f| = P_f$ the projector onto final states (2.4) becomes

$$I(t) = C \sum_{\alpha,\beta} \langle\beta|(\underset{\sim}{e}\cdot\underset{\sim}{D})P_f(\underset{\sim}{e}^*\cdot\underset{\sim}{D})|\alpha\rangle\langle\alpha|\rho(t)|\beta\rangle. \qquad (2.5)$$

From the previous section the evolution of the density matrix is

$$\rho(t) = U(t)\rho(0)U^\dagger(t)$$

with

$$U(t) = \exp(-\frac{i}{\hbar}Ht)$$

and

$$H|\alpha\rangle = \hbar(\omega_\alpha - \frac{i}{2}\gamma_\alpha)|\alpha\rangle.$$

The presence of a phenomenological damping term, γ_α, requires mathematical justification which shall not be given here but see BG 74. γ_α can be taken as the inverse of the lifetime of the state $|\alpha\rangle$. The intensity then becomes

$$I(t) = C \sum_{\alpha,\beta} \langle f|(\underset{\sim}{e}\cdot\underset{\sim}{D})p_f(\underset{\sim}{e^*}\cdot\underset{\sim}{D})|\alpha\rangle\langle\alpha|\rho(0)|\beta\rangle \cdot$$

$$\times \exp[-i(\omega_\alpha-\omega_\beta)t]\exp[-\tfrac{1}{2}(\gamma_\alpha+\gamma_\beta)t] \ . \tag{2.6}$$

This is the fundamental expression for quantum beats. It shows that beats are possible so long as (MG 74)

$$\sum_f \langle\beta|\underset{\sim}{e}\cdot\underset{\sim}{D}|f\rangle\langle f|\underset{\sim}{e^*}\cdot\underset{\sim}{D}|\alpha\rangle \neq 0 \tag{2.7}$$

and

$$\langle\alpha|\rho(0)|\beta\rangle \neq 0 \ . \tag{2.8}$$

The first is the condition that each of the upper states must be able to decay to the same final state via the same transition operator $\underset{\sim}{D}$. The energy structure of final states does not affect the beat pattern. The second is the condition that the initial density matrix in the eigenbasis of H_2 must have off diagonal elements. This is known as the alignment condition.

Certain assumptions about the initial density matrix can significantly simplify the problem. Because the foil interaction takes place in such a short time ($< 10^{-14}$ s) the density matrix may be written in an eigenbasis of H_1 composed of uncoupled atomic states $|LM_L SM_S IM_I\rangle$ if the atom obeys LS coupling. Furthermore in this representation $\rho(0)$ is assumed to be spin independent so that

$$\langle LM_L SM_S IM_I | \rho(0) | L'M_L' SM_S' IM_I' \rangle$$

$$= \delta_{M_S M_S'} \delta_{M_I M_I'} \frac{\langle LM_L | \rho(0) | L'M_L' \rangle}{(2S+1)(2I+1)} .$$

If the foil is perpendicular to the beam, axial symmetry demands that $\rho(0)$ be invariant for any rotation about z-axis chosen as the beam axis. It must also be invariant under reflection in any plane containing the beam. These symmetry conditions lead to (Ma 70)

$$\langle LM_L | \rho(0) | L'M_L' \rangle = \delta_{M_L M_L'} \langle L|M_L| \, |\rho(0)| L'|M_L'|\rangle$$

from which it can be seen that $\rho(0)$ in the H_1 representation is diagonal for a given L. The alignment condition demands that these diagonal elements must not all be the same. This can be shown by writing

$$\langle \alpha | \rho(0) | \beta \rangle = \sum_i \langle \alpha | i \rangle \sigma_i \langle i | \beta \rangle$$

with $\sigma_i = \langle i | \rho(0) | i \rangle$. If σ_i were the same for all

diagonal elements

$$\langle \alpha | \rho(0) | \beta \rangle = \sigma \sum_i \langle \alpha | i \rangle \langle i | \beta \rangle = \sigma \langle \alpha | \beta \rangle = 0$$

since the sets $|\alpha\rangle$ and $|i\rangle$ are taken to span the same subspace. But $\langle \alpha | \rho(0) | \beta \rangle \neq 0$ by (2.8) so not all the σ_i are the same.

As a specific example of this alignment condition consider the $n = 2$ ^2P state of hydrogen in zero field ignoring hyperfine structure. Then

$$\langle 1 \tfrac{1}{2} M_L M_S | \rho(0) | 1 \tfrac{1}{2} M'_L M'_S \rangle =$$

M_L	M_S	M'_L: 1		0		-1	
		M'_S: ½	-½	½	-½	½	-½
1	½	$\sigma_1/2$	0	0	0	0	0
	-½	0	$\sigma_1/2$	0	0	0	0
0	½	0	0	$\sigma_0/2$	0	0	0
	-½	0	0	0	$\sigma_0/2$	0	0
-1	½	0	0	0	0	$\sigma_1/2$	0
	-½	0	0	0	0	0	$\sigma_1/2$

H_2 for this case is the free atom Hamiltonian with LS coupling. The transformation to the J, M_J representation is accomplished with Clebsch-Gordon coefficients:

$$\langle 1 \, \tfrac{1}{2} \, JM_J | \rho(0) | 1 \, \tfrac{1}{2} \, J'M_J' \rangle = \sum_{M_L M_S} \langle 1 \, \tfrac{1}{2} \, JM_J | 1 \, \tfrac{1}{2} \, M_L M_S \rangle$$

$$\times \langle 1 \, \tfrac{1}{2} \, M_L M_S | \rho(0) | 1 \, \tfrac{1}{2} \, M_L M_S \rangle \langle 1 \, \tfrac{1}{2} \, M_L M_S | 1 \, \tfrac{1}{2} \, J'M_J' \rangle \, ,$$

All of these coefficients may be generated from the simple table (CS 63).

$$\langle j_1 \, \tfrac{1}{2} \, m_1 m_2 | j_1 \, \tfrac{1}{2} \, jm \rangle$$

$j =$	$m_2 = \tfrac{1}{2}$	$m_2 = -\tfrac{1}{2}$
$j_1 + \tfrac{1}{2}$	$\sqrt{\dfrac{j_1 + m + \tfrac{1}{2}}{2j_1 + 1}}$	$\sqrt{\dfrac{j_1 - m + \tfrac{1}{2}}{2j_1 + 1}}$
$j_1 - \tfrac{1}{2}$	$-\sqrt{\dfrac{j_1 - m + \tfrac{1}{2}}{2j_1 + 1}}$	$\sqrt{\dfrac{j_1 + m + \tfrac{1}{2}}{2j_1 + 1}}$

After evaluating the coefficients and performing the indicated sum, the transformed density matrix may be written

$$\langle 1 \tfrac{1}{2} J M_J | \rho(0) | 1 \tfrac{1}{2} J' M_J' \rangle =$$

J	M_J \ M_J'	3/2	1/2	-1/2	-3/2	1/2	-1/2
	J' →	3/2				1/2	
	3/2	$\sigma_1/2$	0	0	0	0	0
$\tfrac{3}{2}$	1/2	0	$(\sigma_1+2\sigma_0)/6$	0	0	$(\sigma_1-\sigma_0)/\sqrt{18}$	
	-1/2	0	0	$(\sigma_1+2\sigma_0)/6$	0	0	0
	-3/2	0	0	0	$\sigma_1/2$	0	$(\sigma_0-\sigma_1)/\sqrt{18}$
$\tfrac{1}{2}$	1/2	0	$(\sigma_1-\sigma_0)/\sqrt{18}$	0	0	$(2\sigma_1+\sigma_0)/6$	0
	-1/2	0	0	$(\sigma_0-\sigma_1)/\sqrt{18}$	0	0	$(2\sigma_1+\sigma_0)/6$

This shows by example that off-diagonal elements occur only if $\sigma_0 \neq \sigma_1$. Note too that off-diagonal elements only occur for like values of M_J.

To summarize this section, equations (2.7) and (2.8) represent necessary conditions for quantum beats. Each of the upper states must couple to the same ground state by the same transition operator. The initial density matrix is solely a function of the beam-foil interaction. After considering the short excitation time in the foil, spin independence is postulated and that plus axial symmetry and reflection symmetry leads to a density matrix diagonal in the uncoupled atomic representation. That the diagonal elements are not all equal is the alignment condition verified by the

existence of zero-field quantum beats. The existence of off-diagonal matrix elements in the basis states of H_2 also follows from the sudden perturbation condition (coherence) which for zero field allows the transformation to be made via Clebsch-Gordon coefficients. The density matrix elements, σ_i, are referred to as excitation cross sections since they are dependent only on the foil interaction.

2.4 Zero-field Beats

The existence of zero-field quantum beats was first suggested by Joseph Macek (Ma 69) and first observed by H.J. Andrä (An 70) who followed the suggestion. It should be apparent from the previous section that zero-field beats, with an assumption of no cascades, are amenable to a thorough theoretical treatment since transformations required to evaluate matrix elements involve only well known coupling coefficients. The complications which arise are purely spatial and thorough treatments have been given in the literature, most notable being FM 73, El 73 and BG 74.

Equation (2.5) could be written

$$I(t) \propto tr[M\rho(t)]$$

with M the monitoring operator (CP 66) proportional to

$(e \cdot D)(e \cdot D)^{+}$. If M and ρ were both expanded into spherical tensor operators the various moments of ρ could be related to combinations of different products of J. For example alignment with axial symmetry is the same as a nonzero expectation value of $3J_z^2 - J^2$. If the expectation value of J were nonzero the system would have initial orientation (possible, for example, if axial symmetry were broken). The formalism allows one to relate various combinations of the polarization of the emitted light (Stokes parameters) to the various excitation cross sections permitted by the foil interaction.

To obtain all the parameters of interest experimentally, the emitted radiation should be viewed through a quarter-wave plate and linear polarizer. The polarizer is set parallel, perpendicular and at 45° to the beam and this latter measurement repeated after rotating the quarter-wave plate 45°. This entire set of measurements is then repeated with the optical axis forming a different angle to the beam. Just such a meticulous experiment has recently been performed by Berry et al. (BCES 74) in conjunction with a tilted foil experiment. The results showed a clearly measurable effect on the polarization as the foil angle was changed justifying in principle the need for a more powerful formalism than the one of the

previous section.'

It should be emphasized that with zero-field beats the total intensity is not modulated and the experiment is best performed with a polarizer. This was confirmed by Burns and Hancock (BH 73) who viewed the 2s ^{3}S - 3p ^{3}P 3889 Å radiation from He I. By giving careful consideration to the foil position, they concluded that light polarized parallel to the beam was a pure cosine, twice as intense, and 180° out of phase with light polarized perpendicular to the beam. With the polarizer set to 54.8° relative to the beam axis such that the parallel and perpendicular components were combined in the ratio 1:2, the signal was proportional to the total intensity and was not modulated. These results are in strict agreement with theory which postulates a spin independent foil excitation giving strong support to Macek's analysis. The modulations, then, for zero-field are traced to a reversible exchange of angular momentum between internal degrees of freedom (FM 73).

2.5 Zeeman Beats

The Zeeman effect is the splitting of an atomic level into its component magnetic sublevels by an external uniform magnetic field B. The Hamiltonian

of an atom in such a field is given by

$$H = H_a + \frac{\mu_B}{h}(\underset{\sim}{L} + g_s\underset{\sim}{S})\cdot\underset{\sim}{B} ,$$

with μ_B the Bohr magneton and g_s the factor by which
the electron magnetic dipole moment differs from that
of a classical particle with angular momentum $\underset{\sim}{S}$. If
the field direction is taken as the z-axis the diagonal
matrix elements of L_z and S_z are (Mi 70)

$$\langle LSJM_J|L_z|LSJM_J\rangle = \hbar M_J \frac{L(L+1) + J(J+1) - S(S+1)}{2J(J+1)}$$

$$\langle LSJM_J|S_z|LSJM_J\rangle = \hbar M_J \frac{S(S+1) + J(J+1) - L(L+1)}{2J(J+1)}$$

First order perturbation then gives the splittings of
the energy level

$$\langle \alpha LSJM_J|H|\alpha LSJM_J\rangle = \epsilon(\alpha LSJ) + g_J\mu_B M_J B \qquad (2.9)$$

with

$$g_J = \frac{1}{2}(1 + g_s) + (g_s - 1)\frac{S(S+1) - L(L+1)}{2J(J+1)} .$$

Since $g_s \approx 2$ within 1 part in one thousand

$$g_J \approx \frac{3}{2} + \frac{S(S+1) - L(L+1)}{2J(J+1)} ;$$

written in this form g_J is called the Landé g-factor.
The energy separation between adjacent magnetic sub-
levels from (2.9) is

$$\hbar \omega_L = g_J \mu_B B \quad ,$$

with $\omega_L = 2\pi$ times the Larmor frequency which is the classical precession frequency of a magnetic dipole, with moment $g_J \mu_B$, in an external field.

The necessary conditions to observe quantum beats are satisfied if the beam is subjected to a uniform transverse magnetic field which may extend right to the foil. Due to the longitudinal alignment along the beam direction a magnetic field perpendicular to the beam induces coherence between states with $\Delta M_J = 2$. The light intensity polarized parallel to the beam (if the magnetic field is at right angles to both the beam and the axis of observation) may then be written (MG 74)

$$I(t) = I(0) [1 + A \cos(2\omega_L t)] \exp(-t/\tau) \quad . \qquad (2.10)$$

A measure of the beat frequency gives a measure of the Landé g-factor, a parameter of fundamental importance for determining the validity of the coupling scheme employed for the description of atomic states.

The usual experimental technique employed with Zeeman beats is to observe the beam at a fixed distance from the foil and to linearly change the magnetic field thereby eliminating the exponential decay. In order to maintain a small magnetic field and still observe a sufficient number of oscillations, the chosen

detection position should be as far downstream as possible though not so far that the signal intensity is lost in background noise.

Though Zeeman beats offer the possibility of measuring Landé g-factors for ionization states unattainable by other means, there is one severe drawback to this method being applied to any atom. To produce observable splittings small magnetic fields (∿100 gauss) are employed but for many atoms the splittings so induced are comparable in magnitude to the hyperfine structure caused by the nuclear spin. All experiments performed so far which use equation (2.10) have measured samples with $I = 0$. When $I \neq 0$ the theoretical description becomes very complicated (GCBL 73) and the experimental results of Gaillard et al. differed greatly from their theoretical predictions for 3 out of 4 measured levels.

2.6 Stark Beats

The application of a static electric field produces mixing of states with different ℓ-values for hydrogenic atoms. States with the same n and j quantum numbers are energetically degenerate even in the Dirac theory. However in a now famous experiment Lamb (La 52) measured an energy difference between

the 2s $^2S_{\frac{1}{2}}$ and 2p $^2P_{\frac{3}{2}}$ levels in hydrogen which has

come to be called the Lamb shift. Quantum electro-

dynamics (QED) is able to predict an energy shift

from the Dirac value for all fine structure levels

based on an interaction between the electron and the

quantized radiation field. Measurements of the Lamb

shift, usually performed with resonance techniques,.

are among the most precise in all of physics. The

amazing agreement between these measurements and the

predictions of QED is perhaps the greatest achievement

of quantum mechanics.

The observation of Stark beats with beam-foil

spectroscopy allows direct measurement of the Lamb

shift as a zero field interpolation of energy splitting-

ting obtained at several electric field values. Though

uracy cannot hope to rival that of resonance

ues, it is possible, at least in principle, to

the Lamb shift between levels which are not

table in a variety of hydrogenic ions unavailable

re beam-foil.

The major aspect of our experimental attempt

to measure the Lamb shift between the 4p $^2P_{3/2}$-

$^2D_{3/2}$ levels in boron V by looking at the n = 4 to 3

transition at 749 Å. Fig. 2. is a partial energy

level diagram for boron V excluding hyperfine structure

eV $^2S_{1/2}$ $^2P_{1/2, 3/2}$ $^2D_{3/2, 5/2}$ $^2F_{5/2, 7/2}$

340 — n=∞

330

857 — — 1.42   284 — — 0.45   141

320   51   4

310

— — 3.4   677

2033

300   120   3

290

280

270

6865

260

405   2

250

Values are energy
differences in GHz.

0   1
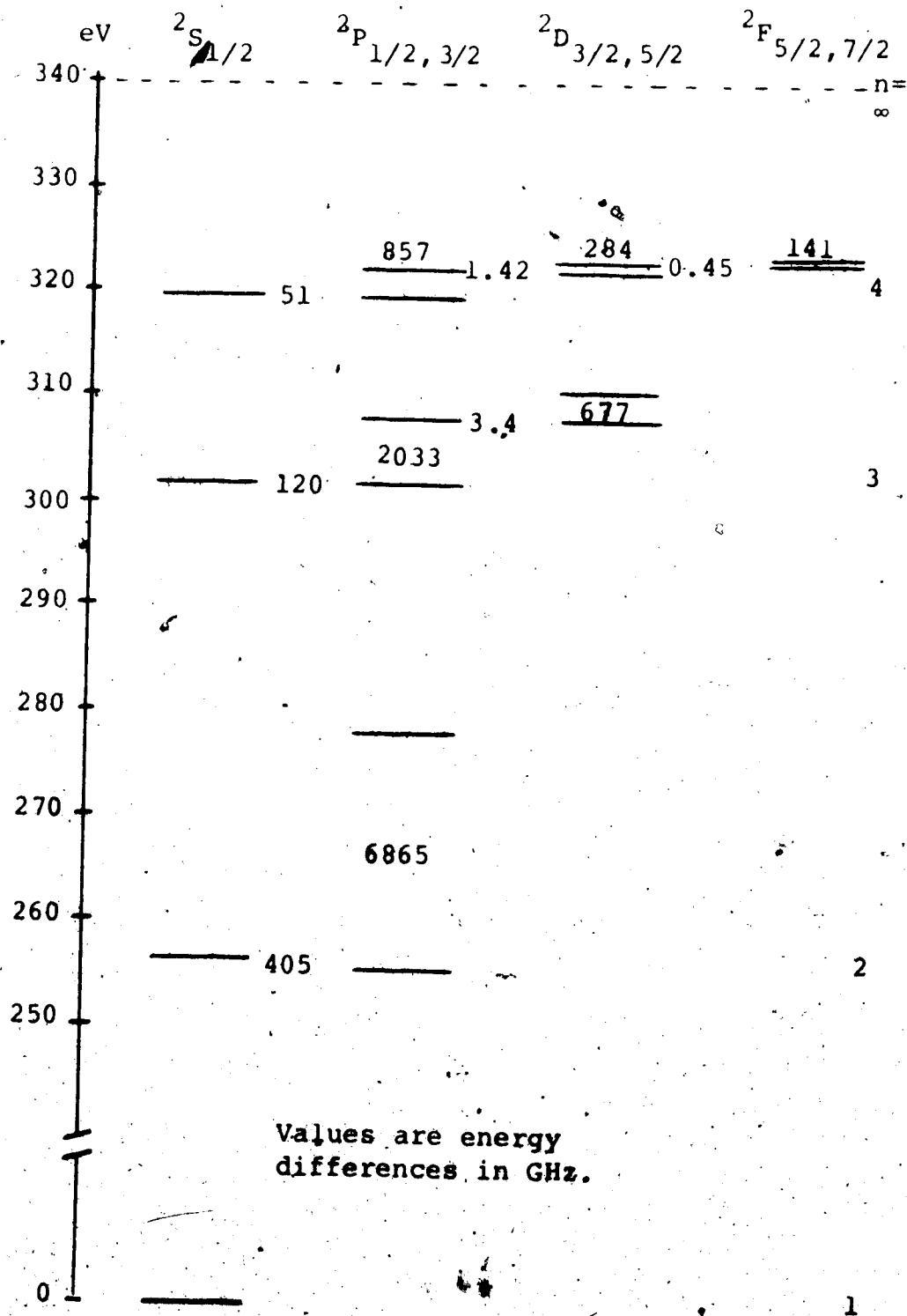
Fig.2. Partial Energy Level Diagram for Boron V
(Scale at left for ground state and $^2P_{1/2}$
levels only).

but including both radiative corrections and corrections for finite nuclear charge distribution and finite nuclear mass. The calculation was performed using the equations compiled by Garcia and Mack (GM 65).

When a hydrogen atom is subjected to an electric field the linear Stark effect produces splittings in the fine structure levels corresponding to different values of $m_{|j|}$. The seven fine structure levels of $n = 4$ split into 16 levels which yield a maximum number of 120 different frequencies! However many of these are nearly identical and most do not fall into the experimental resolution. A program to evaluate the energy levels for given electric field had previously been written here following the procedure of Lüders (Lü 51). The output was used to determine which frequencies might be observable and to plot an extrapolation curve for those that were. The results will be discussed in Chapter V. The possibility that non-linear effects might be important at fields as high as 1000 volts/cm was not considered.

In order to calibrate the external electric field which was axially applied (see Chapter III) the experiment was performed with hydrogen and the Lyman-α transition at 1216 Å was observed. Quantum beats were detected at two different electric field

values and the resulting calibration agreed favorably
with geometrical considerations.

The field calibration with Lyman-α offered an
experimental opportunity to check a different aspect
of Stark beats. Though the frequency patterns in
quantum beats can be quite complicated, in principle
they can be predicted theoretically. Measurements of
frequencies simply confirm theoretical models or in
the case of Zeeman beats ,shed light on the proper
coupling scheme to use. Quantum beat amplitude and
phases however cannot yet be theoretically calculated
since they depend in an unknown manner on the beam-
foil interaction. Most current QB research is directed
toward understanding this interaction. Recently Eck
(Ec 73) proposed an experiment for hydrogen in which
data is collected with an electric field first parallel
then anti-parallel to the beam axis. The experiment
was performed by Gaupp et al. (GAM 74) who interpreted
their results to mean the electron cloud, in zero field,
is displaced in front of the proton as the atom leaves
the foil. It was a simple matter for us to perform
this experiment while at Argonne but unfortunately time
only permitted one set of data to be taken with reversed
electric field.

The discussion in sections 2.3 and 2.4 centered
on quantum beats between levels of a single atomic

term such as ^2P. For all nonhydrogenic atoms the
energy separation between terms is too large to
spatially resolve though not necessarily too large
for coherence to be present. But for hydrogen,
different terms are essentially degenerate and
though symmetry arguments predict a density matrix
initially diagonal in M_L and M_S for given L, there
is no reason, as Macek pointed out (Ma 70) why off-
diagonal elements for different L but like M_L and M_S
could not exist. Two types of coherence may be
distinguished, that involving states with equal
parity such as S-D coherence, and that involving
states with odd parity such as S-P coherence. The
former was actually observed in hydrogen Lyman-β under
zero-field conditions by Burns and Hancock (BH 71).
The latter can only be observed using the Stark effect
which mixes terms of opposite parity.

The relevant portion of the density matrix for
$n = 2$, with M_S suppressed since $M_{\frac{1}{2}} = M_{-\frac{1}{2}}$, is

$$\langle LM_L | \rho(0) | L'M_L' \rangle =$$

L	M_L	M_L'	0	1	0	-1
		L'	0		1	
0	0		σ_s	0	σ_{sp}	0
	1		0	σ_{p1}	0	0
1	0		σ_{sp}^*	0	σ_{p0}	0
	-1		0	0	0	σ_{p1}

Eck claims that the beat intensity is proportional to (Ec 73)

$$I(t) \propto \left(\frac{V}{\omega}\right)^2 \left[\frac{1}{3}(\sigma_{p_0} + 2\sigma_{p_1}) - \sigma_s\right] \cos \omega t$$

$$+ \frac{V\omega_0}{\omega^2 \sqrt{3}} \text{Re } \sigma_{sp} \cos \omega t + \frac{V}{\omega\sqrt{3}} \text{Im } \sigma_{sp} \sin \omega t ,$$

where V is the Stark matrix element (in angular frequency units) coupling the $S_{\frac{1}{2}}$ $m_j = \frac{1}{2}$ and $P_{\frac{1}{2}}$ $m_j = \frac{1}{2}$ states, and $\omega = (\omega_0^2 + 4V^2)^{\frac{1}{2}}$ with ω_0 the Lamb shift. V is simply a constant times the electric field intensity. If data is collected with the field first parallel then anti-parallel to the beam and the beats are added and sub-tracted one obtains:

$$I_+ + I_- \propto 2\left(\frac{V}{\omega}\right)^2 \left[\frac{1}{3}(\sigma_{p_0} + 2\sigma_{p_1}) - \sigma_s\right] \cos \omega t \qquad (2.11)$$

$$I_+ - I_- \propto 2 \frac{V\omega_0}{\omega^2 \sqrt{3}} \text{Re } \sigma_{sp} \cos \omega t + 2 \frac{V}{\omega\sqrt{3}} \text{Im } \sigma_{sp} \sin \omega t .$$
$$\qquad (2.12)$$

If the diagonal elements of ρ are considered known from previous measurements (DAWB 72, AD 73), the amplitude and phase of the difference signal allows evaluation of σ_{sp}. The calculation with results will be presented in Chapter V.

CHAPTER III

EXPERIMENTAL EQUIPMENT AND TECHNIQUES

The data acquisition phase of the quantum beat
experiments used the same experimental arrangement as
has previously been used to collect lifetime data.
The original beam-foil set up is described in Li 71.
The current arrangement contains extensive modifica-
tions from the early work to be found in Li 74 and
IL 75. The description given here will be a brief
overview of all the equipment including mention of the
on-line computer, Texas Instrument 980 A, used for the
first time. The description is that of the University
of Alberta Radiation Research Laboratory and while
facilities at Argonne National Laboratory (US) are
much more extensive, an identical spectrometer and
nearly identical target chamber were used there, so
no separate description of that facility will be given.
Differences where applicable will however be mentioned.

Fig. 3 is a diagram of the experimental
arrangement used here. The particle accelerator is a
2 MV Van de Graaff using radio-frequency excitation of
a chosen source gas. (At Argonne it is a 4 MV Dynami-
tron). Two separate source gas containers, thermo-
mechanically controlled, allow two different samples
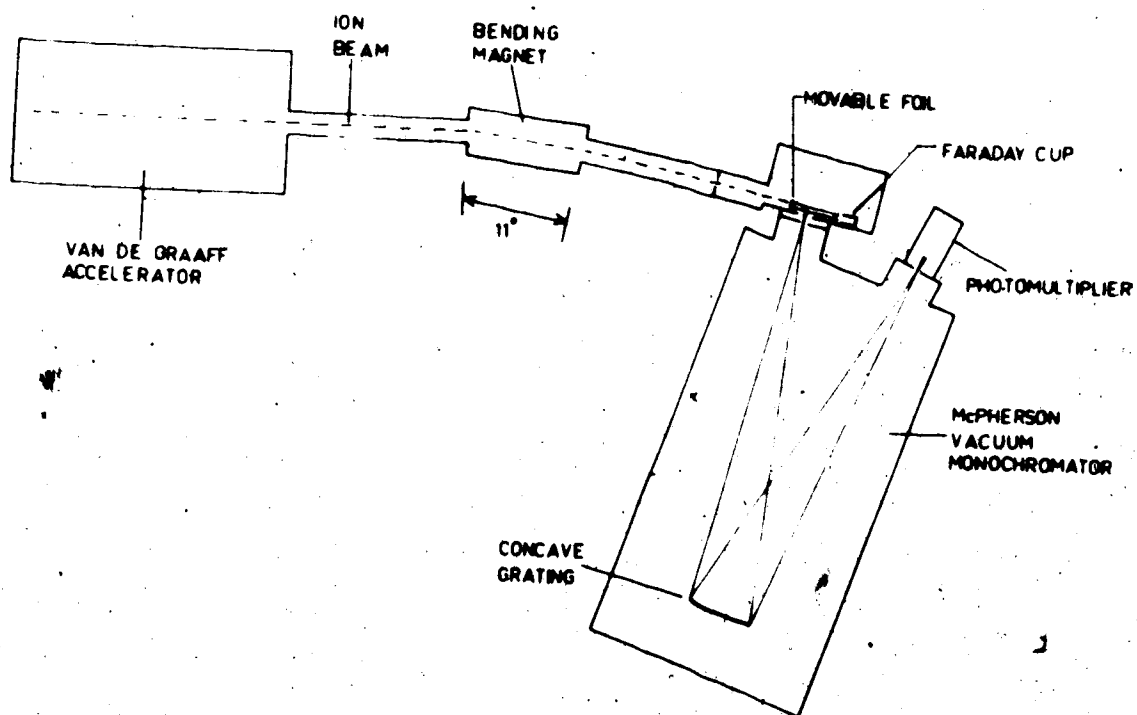
Fig.3 Experimental Arrangement

$$\theta = \frac{w}{d_3} = \frac{s}{d_2}$$

$$d_2 + d_3 = 100 \text{ cm}$$

$$d_1 = 6 \text{ cm}$$
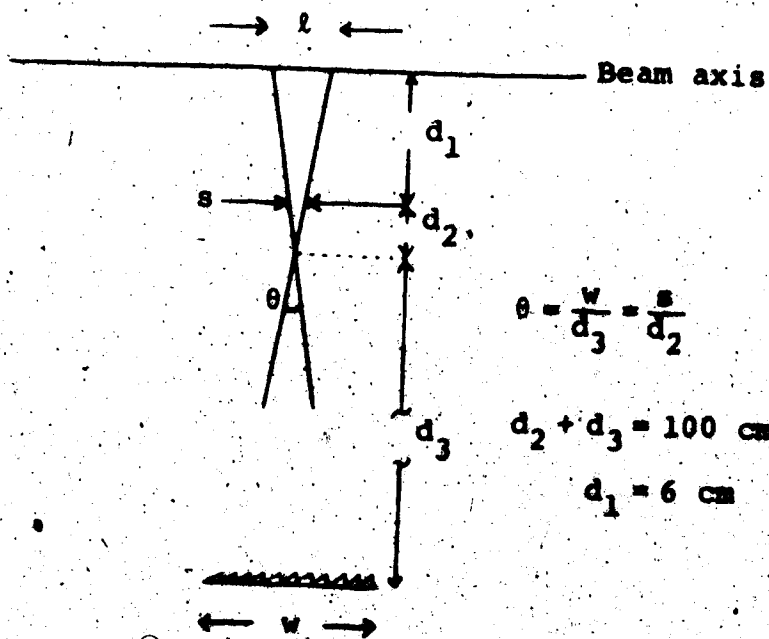
Fig.4 Beam Length Acceptance Geometry

to be studied without opening the machine. Boron trifluoride and hydrogen were used for this experiment. The r-f excitation normally produces singly ionized species and H^+, H_2^+, H_3^+, B^+, BF^+, and BF_2^+ were all observed. Mass separation is accomplished by an electromagnet which deflects the beam 11°. With a full strength field of 5 kilogauss a singly-charged particle of 200 a.m.u. is so deflected. The two stable isotopes of boron, ^{10}B and ^{11}B, were resolved and the more abundant ^{11}B was used for studies at 749 Å.

After deflection in the magnet, the mass-selected ion beam enters the target chamber, which is under reasonably high vacuum (10^{-6} torr). There it passes through a thin carbon foil (5 µg/cm^2) and terminates in a Faraday cup. Beam currents of 1 µA are typical but for boron at Alberta the maximum current was 0.25 µA.

The Target Chambers

Three different target chambers, each with its own advantages and disadvantages, were considered for this experiment; two at Alberta and one at Argonne. Of the two at Alberta one is a focused system, described in Li 71, employing a fixed parabolic mirror and a small rotatable plane mirror. The target foil remains

stationary and the beam is scanned by rotating the
plane mirror. Six foils are mounted on a wheel
allowing targets to be changed without breaking the
vacuum. Presently the mirror coatings are such that
this chamber cannot be used in the far vacuum ultra-
violet region of the spectrum but plans to have the
mirrors platinum coated are being considered. Though
the chamber was mounted and ready for use at the time
of the experiment, the failure of peripheral equipment
forced a change-over to the lifetime chamber used for
mean life studies in the vacuum ultraviolet.

The second chamber at Alberta, used for all
recent mean life studies, is non-focusing and contains
a target holder mounted on a rotating screw. The beam
axis is as close to the spectrometer entrance slit as
possible (6 cm) and the beam is scanned by physically
moving the target upstream. The target moves under
control of a small stepping motor which is geared to
the mounting screw. Control of the motor is handled
remotely by a somewhat sophisticated electronic cir-
cuit, which allows fully automatic or manual control.
Physical position of the gears is visually monitored
with a digital turn count indicator. Variable step
sizes, as small as 0.1 mm, are possible. This target
chamber also allows foils to be changed under vacuum;
as many as 15 foils are available. Though an electric

field can be applied to the beam, the foil changing

mechanism prevents the field from being uniform. .

Experiments involving the use of an electric field

must therefore allow for field calibration.

The target chamber at Argonne, designed with

this experiment in mind, has good electric field

geometry. The foil is mounted across the end of a

small hollow cyclinder which is then inserted into

a large aluminum plate (about 1 cm thick). This large

plate is then mounted to a screw drive which is driven

in the same manner as the one at Alberta. A second

large but thin plate is mounted with insulators 2 cm

downstream from the foil plate and the beam passes

through a small hole in the plate. Opposite potentials

up to 5,000 volts were applied to these plates to

observe Stark-effect quantum beats. Unfortunately .

this chamber could accommodate only one foil at a time.

Spectrometer and Detectors

The spectrometer employed at both Alberta and

Argonne is a McPherson Model 225 one-meter mono-

chromator. The grating used is a Bausch and Lomb

aluminum replica (600 rulings/mm) overcoated with

magnesium fluoride and with platinum. The grating

is concave, 96 mm wide and 56 mm high, blazed at 900 Å

in first order. The entrance and exit slits are at the

radius of curvature of the grating. Since there is
no further focusing, the length of beam from which
light can reach the detector (call it ℓ) is solely a
function of slit width, s, grating width, w, and
distance of the beam axis from the entrance slit, which
as mentioned previously is 6 cm. Since the distance
from slit to grating is one meter, elementary geometry
yields the formula for ℓ (Fig.4):

$$\ell = s + \frac{6(s + w)}{100} \qquad (3.1)$$

By masking the grating, w can be set to any desired
value. At Alberta two masks for grating widths of
10 and 20 mm are frequently used and the option of
changing mask size without opening the spectrometer is
available. The slit width is externally adjusted to
any value with a micrometer screw. Of course, improve-
ment in resolution by masking the grating and narrowing
the slit is paid for by a reduction in light intensity.
For this experiment two combinations were used. The
best resolution was with s = 0.6 mm and w = 10 mm
giving ℓ = 1.2 mm. Some of the boron data were taken
with s = 0.8 mm, w = 20 mm giving ℓ = 2.0 mm.

The detector used below 1100 Å is a Bendix 4210
Spiraltron electron multiplier with no window. The
dark count for this detector is less than 0.1/sec.
Between 1050 Å and 2000 Å an EMR 542 G photomultiplier

with lithium fluoride window is used. Its dark count
is typically 0.4/sec.

Data Collection

Before any data collection actually begins,
several spectral scans at different beam energies in
the wavelength region of interest are recorded. The
spectrometer grating can be turned by hand or with a
built in motor with several available speeds. The
detector output is connected to the pen of a strip-
chart recorder which produces the spectral scan.
Several well-known lines are always available for cali-
bration of the output. Different ionization states are
identified by noting whether the intensity of a line
increases or decreases with changing beam energy. Since
Boron V is hydrogenic, the $n = 4$ to $n = 3$ transition
energy can be easily calculated to be at 749 Å. This
line does not begin to make an appearance until a beam
energy of 1.8 MeV is reached. Once a line has been
selected for study, the spectrometer is left untouched
and data collection begins from a remote control center.

Four parameters specify a given datum during any
one run of a beam-foil experiment; they are,

(1)   foil position, which represents the time since
      ion excitation at the foil

(2)   photon counts, the light intensity integrated
       over the counting time

(3)   counting time, the length of time during which
       the detector signal is accepted by the counter

(4)   integrated beam intensity, the beam current,
       digitized and summed over the counting time.

The stepping motor circuit can be triggered by either
a preset time (time normalization) or a preset current
(current normalization). To compensate for fluctuations
in the beam, current normalization is usually chosen.
Three parameters are then recorded: foil position,
photon counts, and counting time. The latter value is
used to subtract the dark count from the data. Record-
ing of the foil position is most useful for lifetime
experiments in which small steps are used initially,
while larger ones are used near the end of the run.
For quantum beats equal step sizes are used throughout
the run so this parameter becomes redundant.

       Two methods have been used at Alberta for record-
ing the data, but recent developments with the TI 980 A
system promise to improve these methods. The first
employs a Teletype ASR 33 which simultaneously punches
a paper tape and produces a teletype print-out. After
the experiment the paper tape is converted to computer
cards which are edited to remove false starts and
other mistakes, and then run through a data condensation

1

routine which produces cards suitable for analysis

by the program HOMER, as is discussed at the beginning

of ▓▓▓▓▓ chapter. The second method uses a Fabritek

mu▓▓▓▓▓ nalyzer, capable of storing 256 numbers

in ▓▓▓▓ r quarters. Data in the Fabritek, at the

▓m▓▓▓▓ last experiment, could be read by the

▓9▓▓▓ although there was no way to produce an

▓▓▓▓ uitable for the IBM 360/67. Now, however,

▓▓▓▓ ortcoming is soon to be removed and our data

▓▓▓▓ ing methods will be changed accordingly.

O▓▓▓ e Computer

▓▓▓▓ t Alberta a Texas Instrument 980 A computer with

a S▓▓▓ t 700 terminal was used during data acquisition

to pe▓▓▓ rm a preliminary analysis. At the time of the

exp▓▓▓▓ nly a magnetic tape drive was available as

pe▓▓▓▓ equipment and core memory was limited to

16 ▓▓▓ usand bytes. Many routine computer events (such

as compiling a FORTRAN program) were performed by

reading from and writing to two cassette tapes on the

Silent 700. A 100 statement program required 40

minutes to compile. Since then a disk drive has been

added, memory has been increased to 24 K and an X-Y

plotter is operational. Compiling time is now less

than one minute for the previously mentioned program.

The Silent 700 can also now be used as a terminal to

the IBM 360/67 and soon the TI 980 A will be able to read and write MTS files. This final improvement on the system will greatly enhance the Radiation Research facility.

At the Argonne National Laboratory an ASI 2100 computer and peripheral equipment has been functional for several years. All stages of data acquisition, including triggering of the stepping motor, were handled by the computer. Data was collected on magnetic tape, printed with a line printer and punched onto IBM cards before the experiment was concluded. The computer, however, was totally inadequate for any attempt at preliminary data analysis and this contributed to the failure of the experiment. Had it been obvious that there were no quantum beats on data taken at an optimum field voltage with a beam acceptance length of 2 mm, the grating would have been masked and the slit width changed to achieve maximum resolution. This change would have more than doubled the counting time thereby reducing the number of field voltages at which data could be taken. In fact, this change was made, after data had been taken for 1½ hours at five optimum field voltages. It then took 1½ hours to collect data at the highest and lowest field values, the former having too high a beat frequency and the latter too small a beat amplitude to resolve the beats.

Preliminary data analysis for a quantum beat experiment

is most desirable.

CHAPTER IV

METHODS OF DATA ANALYSIS

Two different techniques are discussed in this chapter for analyzing beam-foil quantum beat data. The first is a Fourier transform method and the second is a direct least-squares fit. The analysis was performed on an IBM 360/67 computer and the programs, written in FORTRAN IV, are listed in the appendix. Since the quantum beats appear as small modulations superposed on a multi-exponential background, both of the above techniques enlist the aid of a lengthy program, called HOMER. HOMER was developed here at the University of Alberta between 1970 and 1972 to extract lifetimes from beam-foil data and is briefly described in section 4.1. The data analysis proceeds in two stages. The first is the evaluation of the background using HOMER and the second is the evaluation of the frequency, amplitude and phase of the quantum beat using both the Fourier transform and least-squares methods.

Two short auxiliary programs have also been used to test the success of the analysis methods. The first is one to synthesize data. This uses applicable experimental parameters, up to five background parameters (double exponential plus constant), and up to ten modulation parameters (five frequencies, five

amplitudes and alternately cosine and sine phase). The
second is a program to impart "random" scatter to any
data sample, regardless of whether the data is synthetic
or actual. The program is referred to as the routine,
FUZZ, and has proven especially useful in determining
signal to noise characteristics of a data sample. Of
course, no scatter which is generated within a program
can be truly random and this routine is limited to using
one of five random numbers with which it generates
noise. Which of the five numbers is used is selected
by the user prior to running the program. The magnitude
of the noise is determined by the square root of the
number to be altered. FUZZ was lifted in its entirety
from HOMER where it appears as an optional subroutine,
and is listed in the appendix for the interested reader.

All of the output appearing in this chapter is
artificial, generated by the above mentioned programs.
Whether or not the data was "fuzzed" will be made clear
in the text.

4.1 Finite Discrete Fourier Transform

A useful comparison between the usual and finite
discrete Fourier transform is given in GS 66. The
usual definition for the continuous case is

$$F(k) = \int_{-\infty}^{\infty} f(x) \exp(2\pi ikx)\, dx$$

while for the discrete case

$$F(m) = \sum_{n=1}^{N} f(n) \exp(2\pi inm/N) . \qquad (4.1)$$

N is the total number of data points, $f(n)$ the datum

at position n, while $F(m)$ is the transform. Both n

and m are integers running from 1 to N. To obtain the

inverse transforms one only needs the orthogonality

conditions which for the continuous case is

$$\int_{-\infty}^{\infty} \exp[2\pi ik(x-x')] \, dk = \delta(x-x')$$

while for the discrete case it is

$$\sum_{m=1}^{N} \exp[2\pi im(n-n')/N] = N\delta_N(n-n') \qquad (4.2)$$

where δ_N is the Kronecker delta function with its

argument considered modulo N; that is, $\delta_N(pN) = 1$ for

integer p, otherwise $\delta_N = 0$. The inverse transforms

can easily be obtained in the usual manner yielding for

the discrete case

$$f(n) = \frac{1}{N} \sum_{m=1}^{N} F(m) \exp(-2\pi inm/N) . \qquad (4.3)$$

Note that for the continuous case the usual factor of

2π does not appear outside the integral because of its

inclusion in the exponential. This has been done

deliberately so that k would equal $1/\lambda$, the wavenumber,

commonly used in spectroscopy.

To relate the integers n and m to physical
parameters the arguments of the exponentials must
be related by

$$\frac{nm}{N} = kx = \nu t \qquad (4.4)$$

with t the time since foil excitation, ν the frequency,
k the wavenumber and x = ct; note that x is not the
physical position downstream from the foil. This
physical position (call it x') is related to the beam
velocity, v_B, and the step size, d, by x' = v_Bt = nd.
Therefore

$$x = n \frac{cd}{v_B} = n S_C \qquad (4.5)$$

where S_C is called the scale factor and is constant
over any data set. Typically 0.5 cm $\gtrsim S_C \gtrsim$ 50 cm.
With this value for x eq. (4.4) gives k = $m/N S_C$. The
frequency spectrum is discreet as expected starting at
k(low) = $1/N S_C$. The upper limit would appear to be
m = N but for the fact that the second half of the
transform is, except for phase, the same as the first
half. The upper limit thus occurs at m = N/2. Then
k(high) = $1/2S_C$ which corresponds to each data point
being alternately above and below the background.
Trustworthy results for experiments with fewer than
100 data points are not obtained close to either limit.

The modulations under consideration are superposed
on a background which must be removed before the trans-
form analysis can be performed. Calling this background
Bk(t), the data can be decomposed as

$$Data = R(t) \, Bk(t) + Bk(t)$$

with R(t) the normalized residuals (beat). The only
requirement for Bk is that it be a least-squares
approximation to the data which ignores the modulation.
For this analysis Bk was assumed to be a sum of expon-
entials and its determination was accomplished by the
HOMER routine (IL 74) which can fit a maximum of six
parameters in the following form:

$$Bk(t) = A_1 \exp(-t/\tau_1) + A_2 \exp(-t/\tau_2) + A_3 \exp(-t/\tau_3)$$

where t, as before, is the time since foil excitation
and A_1, τ_1, A_2, τ_2, A_3, τ_3 are determined by the pro-
gram. The optimum number of parameters (between 2 and
6) is that which minimizes the reduced chi-squared.
Criteria for goodness-of-fit as well as a clear over-
all discussion of the multi-exponential data reduction
problem can be found in Li 74.

For computer analysis, sine and cosine functions
are substituted for the complex exponentials in (4.1).
Each are added and then squared to produce a graph of

$F(k)$ $F^*(k)$. The individual sine squared and cosine squared values are printed but not graphed. They are used to determine the phase of the beat as explained in a later paragraph. The individual transforms actually used for data analysis are

$$F_C(k) = \sum_{n=1}^{N} R(n) \cos(2\pi n S_C k) \qquad (4.6a)$$

$$F_S(k) = \sum_{n=1}^{N} R(n) \sin(2\pi n S_C k) \qquad (4.6b)$$

with $F F^* = F^2(k) = F_C^2 + F_S^2$. When evaluating this at a selected set of values for k it is not necessary to restrict the plot to only N/2 points. Intermediate values may be evaluated to produce a smooth transform but the resolution limit is set by the orthogonality condition. If a peak is observed at some value k corresponding to an integer m, then the amplitude will be zero at $m \pm 1$. The half width of the peak is then $\Delta m = 1$ or $\Delta k = 1/NS_C$.

Fig. 5 shows a semilog plot of synthetic data with a cosine beat at 2.25 GHz (5% amplitude) and a background function

$$B(t) = 7000 \exp(-t/0.1 \text{ ns}) + 3500 \exp(-t/0.4 \text{ ns}).$$

This background resembles that of B V at 749 Å. The scale factor corresponding to typical experimental
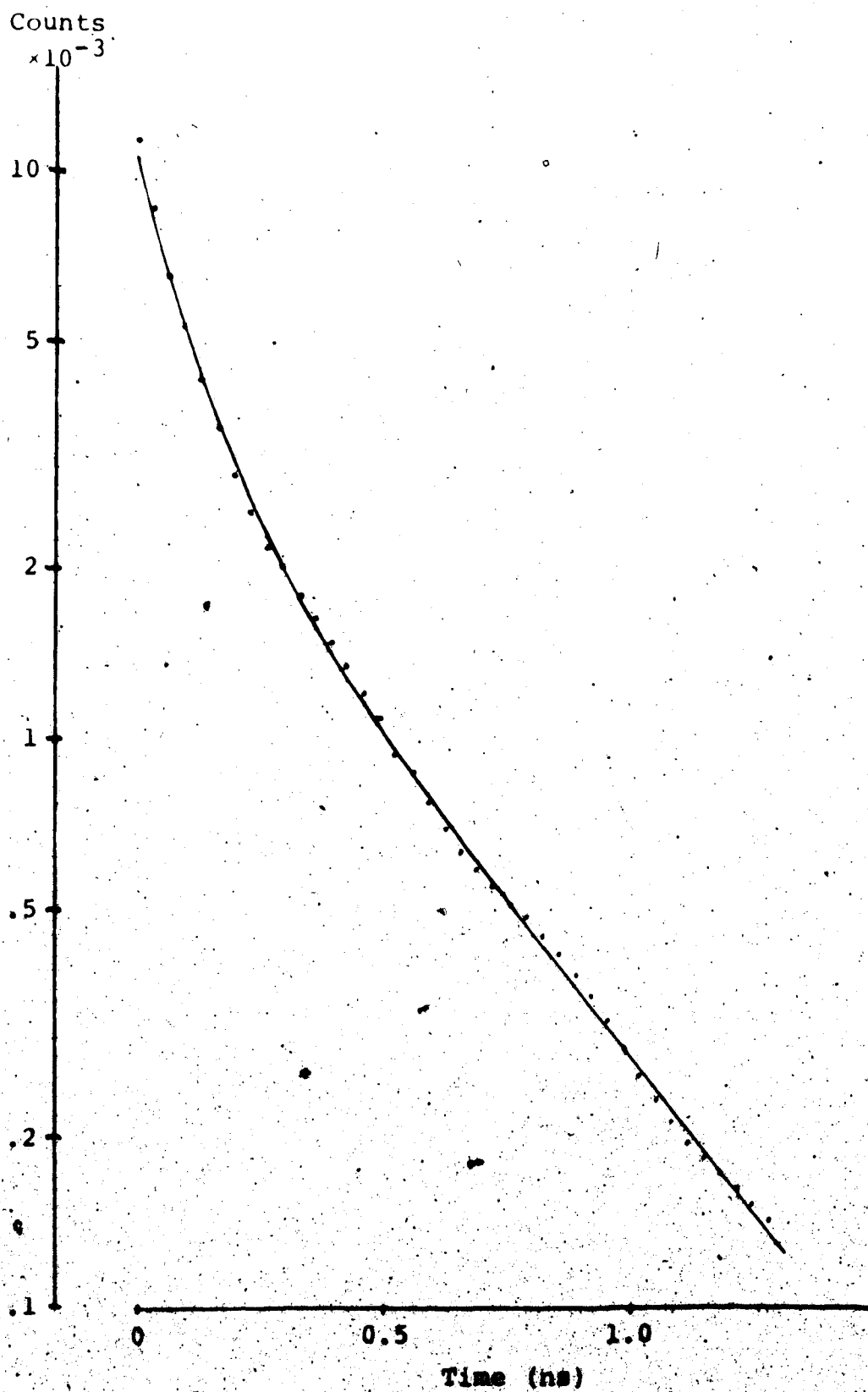
Fig.5 Simulation of Boron V Data

conditions was chosen to be 1.0 cm and 40 points were generated. The resolution is $\Delta k = 0.025 \ cm^{-1}$ which is also the starting frequency corresponding to $m = 1$. Fig. 7 shows the Fourier transform in the low frequency part of the spectrum. The maximum amplitude occurs at $m = 3$ while the amplitude is zero at $m = 2$ (1.5 GHz) and $m = 4$ (3.0 GHz).

4.2 Amplitude and Phase Determination

For sine and cosine functions orthogonality may be written:

$$\sum_{x=1}^{N} \cos(2\pi kx) \cos(2\pi k'x) = \frac{N}{2} \delta_N(k-k')$$

$$\sum_{x=1}^{N} \sin(2\pi kx) \sin(2\pi k'x) = \frac{N}{2} \delta_N(k-k') \qquad (4.7)$$

$$\sum_{x=1}^{N} \sin(2\pi kx) \cos(2\pi k'x) = 0 .$$

Properly the sum is over n not x, and the argument of the Kronecker delta is m not k. Assuming the form of the modulation to be $A \cos(2\pi k'x - \theta)$, (4.6a) gives

$$F_c(k) = \sum_{x=1}^{N} A \cos(2\pi k'x - \theta) \cos(2\pi kx)$$

$$= \sum_{x=1}^{N} A \cos\theta \cos(2\pi k'x) \cos(2\pi kx)$$

$$+ \sum_{x=1}^{N} A \sin\theta \sin(2\pi k'x) \cos(2\pi kx) .$$

SUMSQD	SUMSIN	SUMCOS	FREQU. (GHZ)	ENERGY (CM-1)
0.4091E-03	0.1956E-01	-0.5081E-02	0.750	0.0250
0.1404E-02	-0.1138E-01	-0.3570E-01	0.825	0.0275
0.5594E-02	-0.5733E-01	-0.4804E-01	0.900	0.0300
0.1259E-01	-0.1064E+00	-0.3550E-01	0.975	0.0325
0.2075E-01	-0.1441E+00	0.1034E-02	1.050	0.0350
0.2749E-01	-0.1574E+00	0.5217E-01	1.125	0.0375
0.3001E-01	-0.1403E+00	0.1017E+00	1.200	0.0400
0.2650E-01	-0.9664E-01	0.1310E+00	1.275	0.0425
0.1739E-01	-0.4132E-01	0.1252E+00	1.350	0.0450
0.6278E-02	0.3105E-02	0.7917E-01	1.425	0.0475
0.1523E-03	0.1228E-01	0.1194E-02	1.500	0.0500
0.8556E-02	-0.3202E-01	-0.8678E-01	1.575	0.0525
0.4175E-01	-0.1347E+00	-0.1536E+00	1.650	0.0550
0.1081E+00	-0.2832E+00	-0.1671E+00	1.725	0.0575
0.2115E+00	-0.4481E+00	-0.1033E+00	1.800	0.0600
0.3489E+00	-0.5890E+00	0.4464E-01	1.875	0.0625
0.5097E+00	-0.6641E+00	0.2621E+00	1.950	0.0650
0.6768E+00	-0.6422E+00	0.5142E+00	2.025	0.0675
0.8284E+00	-0.5116E+00	0.7528E+00	2.100	0.0700
0.9428E+00	-0.2853E+00	0.9281E+00	2.175	0.0725
0.1002E+01	0.2734E-03	0.1001E+01	2.250	0.0750
0.9960E+00	0.2938E+00	0.9538E+00	2.325	0.0775
0.9248E+00	0.5409E+00	0.7951E+00	2.400	0.0800
0.7987E+00	0.6977E+00	0.5584E+00	2.475	0.0825
0.6365E+00	0.7419E+00	0.2933E+00	2.550	0.0850
0.4615E+00	0.6772E+00	0.5312E-01	2.625	0.0875
0.2969E+00	0.5319E+00	-0.1187E+00	2.700	0.0900
0.1618E+00	0.3498E+00	-0.1985E+00	2.775	0.0925
0.6712E-01	0.1786E+00	-0.1877E+00	2.850	0.0950
0.1518E-01	0.5671E-01	-0.1094E+00	2.925	0.0975
0.1811E-04	0.4166E-02	-0.8695E-03	3.000	0.1000
0.1006E-01	0.1918E-01	0.9844E-01	3.075	0.1025
0.3158E-01	0.8112E-01	0.1581E+00	3.150	0.1050
0.5225E-01	0.1587E+00	0.1645E+00	3.225	0.1075
0.6369E-01	0.2206E+00	0.1226E+00	3.300	0.1100
0.6274E-01	0.2450E+00	0.5233E-01	3.375	0.1125
0.5107E-01	0.2252E+00	-0.1931E-01	3.450	0.1150
0.3363E-01	0.1703E+00	-0.6794E-01	3.525	0.1175
0.1642E-01	0.1006E+00	-0.7934E-01	3.600	0.1200
0.4396E-02	0.3948E-01	-0.5326E-01	3.675	0.1225
0.3428E-04	0.5425E-02	-0.2201E-02	3.750	0.1250
0.2944E-02	0.6272E-02	0.5389E-01	3.825	0.1275
0.1042E-01	0.3728E-01	0.9502E-01	3.900	0.1300
0.1869E-01	0.8378E-01	0.1080E+00	3.975	0.1325
0.2430E-01	0.1269E+00	0.9050E-01	4.050	0.1350
0.2527E-01	0.1506E+00	0.5098E-01	4.125	0.1375
0.2154E-01	0.1467E+00	0.5124E-02	4.200	0.1400
0.1472E-01	0.1175E+00	-0.3025E-01	4.275	0.1425
0.7380E-02	0.7430E-01	-0.4311E-01	4.350	0.1450

FIG.6. FOURIER TRANSFORM OUTPUT OF FIG.5. DATA

```
FREQU.              AMPLITUDE OF FOURIER TRANSFORM
(GHZ)     0..........1.........2.........3.........4.........5
0.750     *
0.825     *
0.900     *
0.975     *
1.050     *
1.125     *
1.200     *
1.275     *
1.350     *
1.425     *
1.500     *
1.575     *
1.650     .*
1.725     .    *
1.800     .       *
1.875     .          *
1.950     .             *
2.025     .               *
2.100     .                  *
2.175     .                    *
2.250     .                     *
2.325     .                     *
2.400     .                    *
2.475     .                  *
2.550     .               *
2.625     .            *
2.700     .         *
2.775     .      *
2.850     .  *
2.925     *
3.000     *
3.075     *
3.150     *
3.225     .*
3.300     .*
3.375     .*
3.450     .*
3.525     .*
3.600     *
3.675     *
3.750     *
3.825     *
3.900     *
3.975     *
4.050     *
4.125     *
4.200     *
4.275     *
4.350     *
```
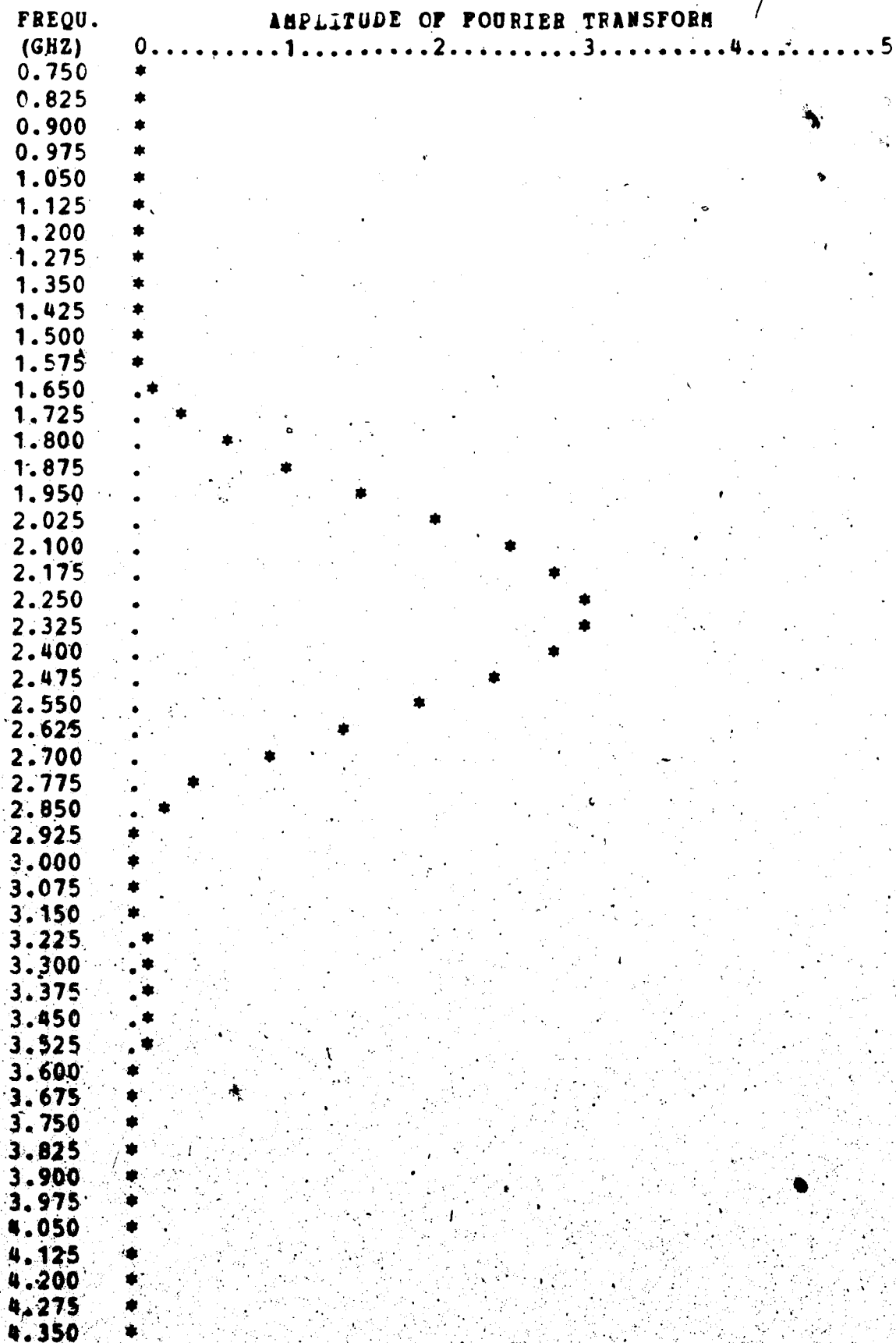
FIG.7.   FOURIER TRANSFORM PLOT OF FIG.5. DATA

Using (4.7) $F_c(k) = (N/2) A \cos \theta$ at $k = k'$. In like fashion $F_s(k) = (N/2) A \sin \theta$ at $k = k'$. So

$$\theta = \arctan(F_s/F_c) \tag{4.8a}$$

and

$$A = \frac{2}{N} (F_c^2 + F_s^2)^{\frac{1}{2}} . \tag{4.8b}$$

The amplitude and phase of the modulation can then be determined from the computer printout values of SUMSIN, SUMCOS, and SUMSQD at a maximum in the graph of the transform.

Several factors contribute errors to an amplitude and phase determined in this manner. A glance at Fig. 6 shows that the phase of the beat is $0°$ at 2.25 GHz but is $-17°$ and $+18°$ at adjacent printed values corresponding to $\Delta m = \mp 1/10$; this is for synthetic, noise free data. The analysis is phase sensitive. This coupled with an inherent uncertainty in the foil position makes absolute phase determination with the transform method uncertain by about $50°$.

Another factor which contributes difficulties affects the amplitude for low frequencies. By low is meant perhaps 2 to 7 complete beats in a data sample. The background fit can be sufficiently distorted by the presence of beats to reduce the amplitude by as much as 20%. Data was synthesized (noise free) with a single beat of known amplitude and frequencies

corresponding to 2, 3, 4, 5 and 7 complete oscillations over the data sample. The data was then transformed twice; first with the known background (same exponential as before) then after being HOMER fitted. This was done separately for a cosine and sine beat. The results for the HOMER fit are shown in Table 1. In all cases the amplitude error using the true background function was less than 0.2%. The last two entries in the table are for a data sample with two beats, one a sine the other a cosine. In all cases the cosine beat had a much larger amplitude error than the sine for equal frequencies. The error also decreases with higher frequency beats to a minimum of about 2%.

Table 1

Beat Amplitudes After HOMER Fit

(True amplitude is 5%)

Frequency (GHz)	Number of Oscillations	Beat Amps. in Percent Cosine	Sine
1.5	2	3.96	4.77
2.25	3	4.17	4.95
3.0	4	4.45	4.91
3.75	5	4.59	4.91
5.25	7	4.75	4.90
3.0/5.25	4/7	4.30	4.60
5.25/3.0	7/4	4.76	4.62

Another source of significant error to the beat
amplitude is due to averaging over a finite length of
beam. This discussion will begin with a single
modulation superposed on a background of one exponen-
tial. It will then be expanded to include a background
of any number of exponentials and the correction factor
so obtained can be applied to any number of modulations.

Let the assumed intensity be of the form

$$y(x) = Bk(x) \ A \ \cos(ax-\theta) + Bk(x) \qquad (4.9)$$

with $Bk(x) = B \exp(-bx)$. It is somewhat more convenient
to use the variable x rather than the time, t, since
foil excitation. Then

$$x = v_B t$$

$$a = \frac{2\pi v}{v_B}$$

$$b = 1/(v_B \tau)$$

with v the frequency of modulation and τ the lifetime
of the excited state. Then the integrated intensity is

$$I(x) = \int_{x-\Delta}^{x+\Delta} y(x') \ dx' \qquad (4.10)$$

with 2Δ being the observed beam length which is dictated
by the geometry of the system. First consider the inte-
gral of the background:

$$\int_{x-\Delta}^{x+\Delta} Bk(x') \ dx' = B' e^{-bx} = Bk'(x)$$

where

$$B' = \frac{2B \ \sinh(b\Delta)}{b} \ .$$

The integral of the first term of (4.9) is:

$$\int_{x-\Delta}^{x+\Delta} Bk(x') \ A \ \cos(ax'-\theta) \ dx' =$$

$$\frac{2B \ e^{-bx} \ A}{(a^2+b^2)} \{\cos(a\Delta) \ \sinh(b\Delta)[b \ \cos(ax-\theta)-a \ \sin(ax-\theta)]$$

$$+ \sin(a\Delta) \ \cosh(b\Delta)[b \ \sin(ax-\theta)+a \ \cos(ax-\theta)]\}.$$

This can be simplified and expressed in terms of B'
as

$$I(x) - Bk'(x) = B' \ e^{-bx} \ C(a,b,\Delta) A \ \cos(ax-\theta'),$$

$$(4.11)$$

with

$$C(a,b,\Delta) = \frac{[\cos^2(a\Delta) + \sin^2(a\Delta) \ \coth^2(b\Delta)]^{\frac{1}{2}}}{[1 + (a\Delta)^2/(b\Delta)^2]^{\frac{1}{2}}} \qquad (4.12)$$

and $\theta' = \theta + \delta + \epsilon$. These phase factors are

$$\tan \delta = b/a$$

$$(4.13)$$

$$\tan \epsilon = -\cot(a\Delta) \ \tanh(b\Delta) \ .$$

I(x) represents the data while Bk'(x) is the background fit. As explained previously the background is subtracted from the data and this difference is divided by the background. $C(a,b,\Delta)$ is then the correction factor to the amplitude. For both $a\Delta$ and $b\Delta << 1$, $C = 1$ as expected. The condition that $a\Delta$ be small is that the averaging length be a small fraction of the beat wavelength. For $b\Delta$ to be small the exponential background must not decay too rapidly. Ideally both of these conditions should be met but in practice, especially with non-focused optics, this is generally not the case. Before considering some typical values let the background be a sum of exponentials:

$$Bk(x) = \sum_n B_n \exp(-b_n x) .$$

Then

$$\int_{x-\Delta}^{x+\Delta} Bk(x') = \sum_n B_n' \exp(-b_n x) \equiv Bk'(x)$$

with

$$B_n' = \frac{2B_n \sinh(b_n \Delta)}{b_n} .$$

For this case

$$I(x) - Bk'(x) = \sum_n B_n' e^{-b_n x} C_n(a,b_n,\Delta) A \cos(ax-\theta') , \quad (4.14)$$

with C_n defined as before with b replaced by b_n. Here

the added condition that $\theta = \theta'$ has been used. It will be shown subsequently that this holds approximately under "usual" experimental conditions. (4.14) shows that normalization hopelessly muddles the picture unless all the C_n are approximately equal. This is in fact the case for $a\Delta < \pi/2$ but differences rapidly become too large to ignore as $a\Delta$ approaches π.

If in addition there is more than one modulation the expression for the residuals becomes

$$I(x) - Bk'(x) = \sum_{n,m} B_n' e^{-b_n x} C_{nm}(a_m, b_n, \Delta) A_m \cos(a_m x - \theta_m')$$

$$(4.15)$$

and a correction factor exists for each A_m.

Since 2Δ is the averaging length, $a\Delta = \pi$ corresponds to a length of one wavelength and the condition that $a\Delta < \pi/2$ is almost mandatory for a meaningful correction to the beat amplitude. For this experiment $\Delta = 0.6$ mm which gives $a\Delta = 1.1$ for hydrogen and $a\Delta = 1.4$ (typically) for boron V. For hydrogen which has a moderate single exponential background, $b\Delta = .05$ while for boron V with a steep double exponential $b_1\Delta = 1.0$ and $b_2\Delta = 0.25$. With these numbers it is possible to show the behavior, under somewhat extreme conditions, of $C(a,b,\Delta)$ and θ'.

The phase shift introduced by averaging over a finite length of beam is $\theta - \theta' = \delta + \epsilon$. From (4.13)

$$\lim_{a\Delta \to 0} (\delta + \epsilon) = 0$$

regardless of $b\Delta$. For $a\Delta = \pi$ this phase shift is about $\pi/2$ for any value of $b\Delta$. Table 2 illustrates some intermediate values. That $\theta' \approx \theta$ for $a\Delta < \pi/2$ and $b\Delta < 1$ is seen to hold.

Table 2

Beam Averaging Phase Shift

	$\theta - \theta'$		
$a\Delta$	$b\Delta = .05$	$b\Delta = .25$	$b\Delta = 1.0$
0	0	0	0
$\pi/4$	0.8°	4°	15°
$\pi/2$	2°	9°	32°
π	91°	95°	108°

Fig. 8 is a set of graphs of $C(a,b,\Delta)$ vs $a\Delta$ for three different values of $b\Delta$ (the same ones as in Table 2). For $a\Delta < \pi/2$ C is insensitive to $b\Delta$ justifying its use as a single correction factor even for a multi-exponential background. For $a\Delta > \pi/2$ this is not the case and a straightforward correction to the beat amplitude is not possible.
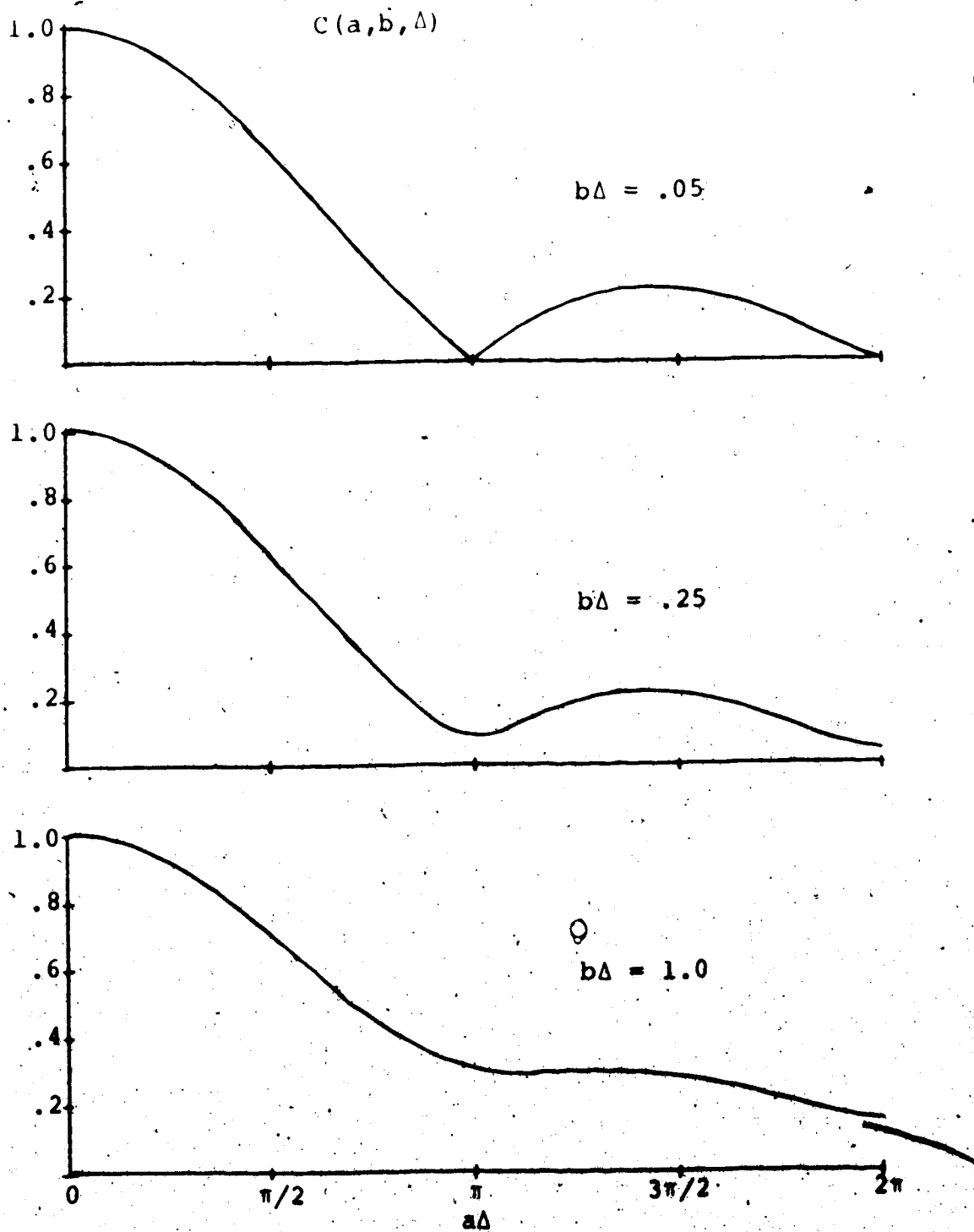
Fig. 8   Beat Amplitude Correction Factor

The analysis considered so far is still deficient
for determining absolute values of beat amplitude. The
integrated intensity as given by (4.10) should be
replaced by

$$I(x) = \int_{x-\Delta}^{x+\Delta} R_s(x') \, y(x') \, dx'$$

with R_s the proper response function of the experimental
apparatus. However frequently only relative amplitudes
of several beats appearing in the Fourier transform are
desired. For this (4.15) with the modified version of
(4.12) supplies the necessary caution that the relative
amplitudes appearing in the transform are not the
relative amplitudes of the beats as well as an expression,
valid under broad but restricted conditions, to correct
for this.

4.3 Least-Squares Evaluation of Amplitude and Phase

A second method to determine the amplitude and
phase of a modulation superposed on a multi-exponential
background was developed using a straightforward
linear least-squares fit. For linearity the frequency
is held constant and input at the value given by the
Fourier transform, but the program is inexpensive
enough to scan a selection of frequencies and produce
a plot much like the transform method. The advantage

over the transform method is that uncertainties in both
amplitude and phase can be evaluated and the reduced
chi-squared with and without a modulated background
can be compared. At present this program is limited
to a single frequency modulation but expansion to
include up to five frequencies (10 parameter fit) should
not be difficult (and should be completed prior to the
next experiment).

The method of least-squares is to minimize chi-squared, the weighted sum of the squares of the devia-
tion between the data and the fitting function. That
is,

$$\chi^2 = \sum_{i=1}^{N} \frac{1}{\sigma_i^2} [y_i - y(x_i)]^2$$

with y_i the datum at x_i, $y(x_i)$ the fitting function,
and σ_i the uncertainty in the datum which for photon
counting experiments is taken to be the square root of
the datum, assuming Poisson statistics. The fitting
function is given by

$$y(x_i) = Bk(x_i) + Bk(x_i) [A_1 \cos(ax_i) + A_2 \sin(ax_i)] .$$

Here $Bk(x_i)$ is the background fit as determined by the
HOMER routine, a is proportional to the assumed known
frequency and A_1 and A_2 are parameters to be determined.
For these the amplitude and phase relative to a cosine

modulation are easily determined from elementary relations.

Setting the partial derivatives of χ^2 with respect to A_1 and A_2 equal to zero leads to the linear equations:

$$f_j = \sum_{k=1}^{2} \alpha_{jk} A_k$$

with

$$f_j = \sum_{i=1}^{N} \left[\frac{1}{\sigma_i^2} (y_i Bk(x_i) - Bk(x_i)^2) \begin{pmatrix} \cos(x_i) \\ \sin(x_i) \end{pmatrix} \right]$$

and j is the column index while

$$\alpha_{jk} = \sum_{i=1}^{N} \frac{Bk(x_i)^2}{\sigma_i^2} \begin{pmatrix} \cos^2(x_i) & \cos \cdot \sin \\ \cos \cdot \sin & \sin^2(x_i) \end{pmatrix}$$

Written this way it is clear how to expand the technique to more than 2 parameters. Note that it is the data itself which is fit and not the normalized residuals. In this way α^{-1} is the error matrix and the uncorrelated uncertainties in A_j are just $\sigma_{A_j}^2 = \alpha_{jj}^{-1}$ (Be 69).

A_1 and A_2 are obtained in the usual way and these are readily converted to a cosine amplitude and phase. The uncertainties in the parameters A and θ with

$$A \cos(ax-\theta) = A_1 \cos(ax) + A_2 \sin(ax)$$

$$A^2 = A_1^2 + A_2^2$$

$$\theta = \tan^{-1}(A_2/A_1)$$

are related to the uncertainties in A_1 and A_2 by

$$\sigma_A^2 = \sigma_{A_1}^2 \left(\frac{\partial A}{\partial A_1}\right)^2 + \sigma_{A_2}^2 \left(\frac{\partial A}{\partial A_2}\right)^2 + 2\sigma_{A_1 A_2}^2 \left(\frac{\partial A}{\partial A_1}\right)\left(\frac{\partial A}{\partial A_2}\right)$$

with $\sigma_{A_1 A_2}^2 = \alpha_{12}^{-1}$, and similarly for θ.

Fig. 9 shows an abbreviated output of this program for the same synthetic data as Fig. 5. The most obvious difference between them is that the graph of the least-squares output does not go to zero at 1.5 and 3.0 GHZ since there is no orthogonality condition for this method. The beat frequency is decided by a minimum in the reduced chi-squared rather than the position of maximum amplitude since these two criteria do not necessarily agree. Reduced chi-squared is simply chi-squared divided by the number of degrees of freedom for the fit. This number is the number of data points less the number of fitting parameters which should include the number of HOMER parameters even though these are not being varied. How close the reduced chi-squared is to one is an indication of the goodness-of-fit. Using this criterion one can obtain

```
CHISQ  FREQU        BEAT AMPLITUDE IN PERCENT
(RED)  (GHZ)   0....1....2....3....4....5....6....7....8
2.19   0.750   .
2.16   0.825   .
2.11   0.900   .
2.06   0.975   .
2.01   1.050   .
1.96   1.125   .
1.91   1.200   .
1.86   1.275   .
1.81   1.350   .
1.75   1.425   .
1.68   1.500   .
1.58   1.575   .
1.44   1.650   .
1.25   1.725   .
1.03   1.800   .
0.79   1.875   .
0.55   1.950   .
0.32   2.025   .
0.15   2.100   .
0.04   2.175   .
0.00   2.250   .
0.04   2.325   .
0.13   2.400   .
0.28   2.475   .
0.46   2.550   .
0.66   2.625   .
0.87   2.700   .
1.07   2.775   .
1.25   2.850   .
1.38   2.925   .
1.47   3.000   .
1.54   3.075   .
1.60   3.150   .
1.65   3.225   .
1.70   3.300   .
1.75   3.375   .
1.81   3.450   .
1.87   3.525   .
1.93   3.600   .
1.98   3.675   .
2.01   3.750   .
2.04   3.825   .
2.06   3.900   .
2.08   3.975   .
2.11   4.050   .
2.13   4.125   .
2.16   4.200   .
2.20   4.275   .
2.23   4.350   .
```

FIG. 9.   LEAST-SQUARES PLOT OF FIG. 5. DATA

the "best" values for frequency, amplitude and phase

with uncertainties in each. It must be mentioned

that if more than one frequency were present on the

data, even widely separated frequencies, the answers

obtained with this method would be incorrect since

the reduced chi-squared would never be close to one.

A least-squares fit with as many frequencies as are

present on the transform must initially be used. The

complementary nature of these two techniques thus

becomes apparent. While the transform method gives

an indication of the amplitude and phase for several

frequencies it offers no indication of the reliability

of the results. Least-squares gives a clear criterion

for goodness-of-fit but becomes increasingly complicated

as more than one frequency are fit.

CHAPTER V

RESULTS AND CONCLUSION

Before the analysis of any beam-foil data involving time-of-flight information, the beam velocity must be determined. Two methods are usually used. The first relies on the energy calibration of the accelerator and compensates for energy loss in the foil using published tables (NS 70). The second is a direct independent measurement of the velocity usually invoking the Doppler shift of a spectral line. This involves a specially designed target chamber with an arrangement of mirrors which has been described elsewhere (Li 71). The first method was applied to all elements examined during the Spring 1974 experiment at Alberta since previous Doppler shift measurements indicated an accuracy of the beam velocity to within 2%. The energy loss for hydrogen and boron at the beam energies employed was less than 1% and this correction was never applied to the quantum beat data since it was not justified by the results. Highly accurate quantum-beat frequency determination can only be obtained by comparing two observed frequencies, one of which is assumed accurately known from other theoretical or experimental evaluation.

5.1 Electric Field Calibration

The target chamber at Argonne National Laboratory was designed specifically to yield a uniform, longitudinal electric field along the beam axis. Calibration was accomplished by measuring the frequency of quantum beats observed in hydrogen Lyman-α emission (1s-2p at 1216 Å). H_3^+ was accelerated to 1.0 MeV and a double foil was used, the first to dissociate the molecule into three protons. Fig. 10 is a semi-log plot of the data at -1,000 volts and Fig. 11 is its Fourier transform. Measurements were taken at three different plate voltages and these with the observed frequencies and their uncertainties are given in Table 3. The uncertainties are solely the statistical estimates given by the least-squares routine. The 2% uncertainty in the beam velocity is greater than any of these. A calibration curve for Ly-α was calculated as mentioned in section 2.6. The field strengths for these three points are shown in Table 3. The first two points agree that the electric field is 6% higher than the plate voltage divided by the 2 cm separation. The agreement indicates a systematic error which can be fully accounted for by the beam velocity uncertainty and the power supply voltage tolerance.
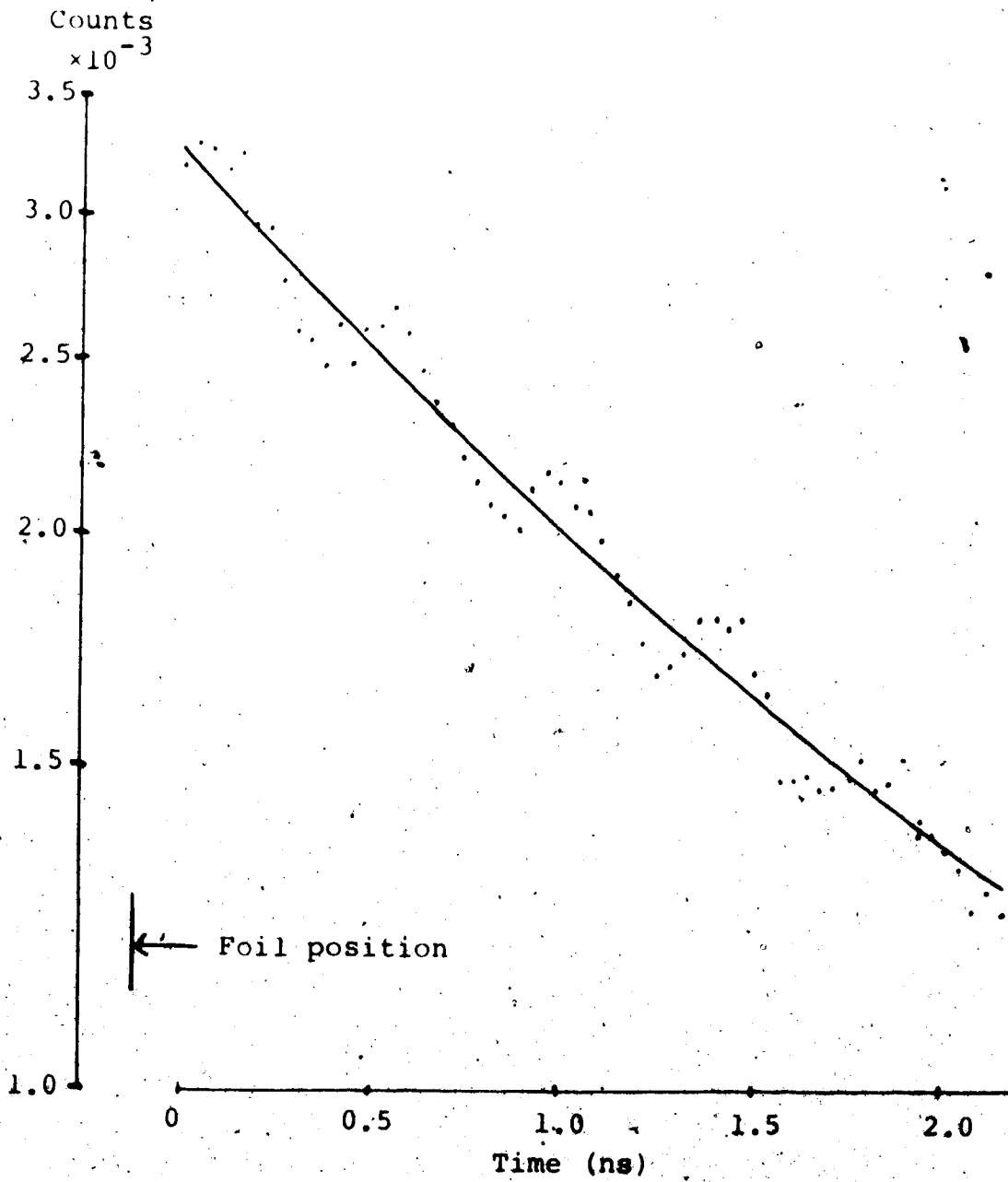
Fig.10 Actual Hydrogen Lyman-α Data

```
FREQU.            AMPLITUDE OF FOURIER TRANSFORM
(GHZ)    0.........1.........2.........3.........4.........5
0.450    *
0.540    .*
0.630    .*
0.720    .*
0.810    *
0.900    *
0.990    *
1.080    *
1.170    *
1.260    *
1.350    *
1.440    *
1.530    .*
1.620    .  *
1.710    .    *
1.800    .   *
1.890    .*
1.980    .*
2.070    .      *
2.160    .         *
2.250    .
2.340    .
2.430    .
2.520    . *
2.610    .
2.700    .
2.790    .
2.880    . *
2.970    *
3.060    *
3.150    .*
3.240    .*
3.330    .*
3.420    .*
3.510    .*
3.600    *
3.690    *
3.780    .*
3.870    *
3.960    *
4.050    .*
4.140    *
4.230    *
4.320    *
4.410    *
4.500    *
4.590    *
4.680    *
4.770    *
```
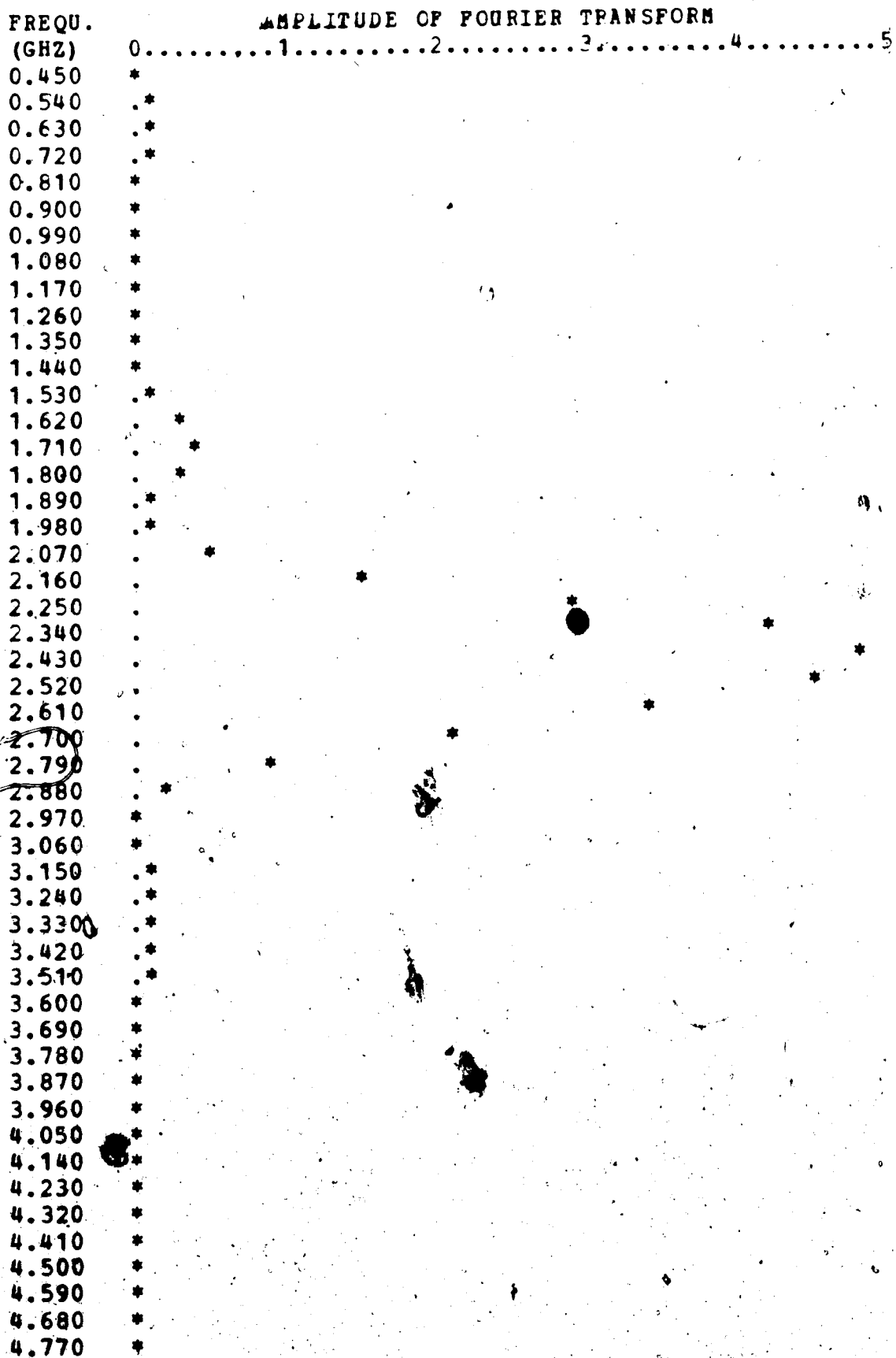
FIG.11.   FOURIER TRANSFORM OF FIG.10. DATA

Table 3.

Quantum Beat Frequencies for Lyman-α

Plate Voltage (Grounded Foil)	Frequency (GHz)	Uncertainty	Field Strength (volts/cm)
-1,000	2.44	±.01	530 ± 3
-2,000	4.53	±.05	1060 ± 14
-4,000	(8.0)	(±.1)	(1970 ± 30)

The figures for -4,000 volts appear in parenthesis since the beat amplitude was so small that it hardly appeared on the Fourier transform. The least-squares routine gave the tabulated frequency with a reduced chi-squared of 1.02 compared to 1.15 without any modulation. The small beat amplitude is a result of averaging over one beat length. At this frequency $a\Delta = 3.76$ and Fig. 8 claims that the beat amplitude will be reduced over 90%.

5.2 Results with Boron

Boron III 2066 Å

The $2s\ ^2S_{\frac{1}{2}} - 2p\ ^2P_{\frac{1}{2},\frac{3}{2}}$ transition of boron III at 2066 Å was examined for zero-field quantum beats at 0.6 and 1.0 MeV. ^{10}B and ^{11}B were individually analyzed after taking data samples with 80 points

separated by 1.0 mm. No polarizer was used and the line was sufficiently intense to collect good statistics. The decay was a single exponential with a lifetime of 5.5 ns which at the lower beam energy corresponds to 18 channels. ^{10}B has a nuclear spin, $I = 3$ while ^{11}B has $I = 3/2$. The calculated hyperfine structure frequencies fall well within experimental resolution but no beats were consistently detected at both beam energies. Also no observed beats had relative frequencies consistent with theory.

It might be premature to conclude that no beats are on the data. Since multiple frequencies are expected, the least-squares program could not be used. Furthermore only F value intervals corresponding to $J = 3/2$ were calculated. Since the fine structure is not optically resolved (34.1 cm^{-1}) and is small enough for coherence to be present, $J = 1/2$ should also be considered. The theoretical frequency pattern could be much more complicated than the one we employed. This data will be among the first analyzed by the expanded version of the least-squares routine and if the analysis clearly indicates the existence of beats a detailed theoretical investigation of the hyperfine structure will be undertaken.

Boron V 749 Å

Data at 749 Å (n = 4 to n = 3) for ^{11}B V was collected at Argonne National Laboratory at 7 different plate voltages between -1,000 and -5,000 volts. Beam energies of 3.2 or 3.0 MeV were used. Typically each data sample represents six scans along the beam with 43 points per scan. Each point was spatially separated by 0.27 mm which represents a temporal separation of about .04 ns. Each scan was added with the on-line ASI 2100 computer. Table 4 lists some of the relevant parameters for each data sample. The lowest and highest plate voltages were taken last at the lower beam energy in an effort to improve the statistics by using higher beam current.

Table 4

Experimental Parameters for Boron V 749 Å

Plate Volt. (volts)	Beam Vel. (mm/ns)	Scale Factor (cm)	Aver. Length (mm)	Statistics
-1,000*	7.25	1.13	1.2	2.4
-2,000	7.49	1.10	2.0	2.0
-2,500	7.49	1.10	2.0	2.0
-3,000	7.49	1.10	2.0	2.0
-3,500	7.49	1.10	2.0	2.0
-4,000	7.49	1.10	2.0	2.0
-5,000*	7.25	1.13	1.2	2.2

*Beam energy 3.0 MeV, otherwise 3.2 MeV.

The fourth column of Table 4 lists the beam averaging length as described in Chapter III. The first and last data sample used a larger grating mask and smaller slit width than did the others. The frequency whose wavelength equals the averaging length is 3.75 GHz for 2.00 mm and 6.04 GHz for 1.2 mm at the listed velocities. These represent the practical upper frequency limits which are considerably smaller than $1/(2S_c) \approx 13.5$ GHz. Counting time for the two data samples with higher resolution was twice as long as for the others and still fewer counts per datum were collected. This is represented by the "Statistics" column which is the mean value over a data sample of the square root of a count divided by the count.

A simplistic but reasonable assertion might be that one cannot detect beats of amplitude less than the statistics of the data sample. As a generality this is not true since the noise level of a Fourier transform depends on how many data points have been collected. However, for 43 points, the assertion appears correct based on studies of synthetic data which were "fuzzed" as described in the previous Chapter. Figs. 12 to 14 show the Fourier transforms of synthetic data with three widely separated frequencies. The data was carefully generated to duplicate

```
FREQU.              AMPLITUDE OF FOURIER TRANSFORM
 (GHZ)     0.........1.........2.........3.........4.........5
 0.600     *
 0.750     *
 0.900     .*
 1.050     .*
 1.200     *
 1.350     ..*
 1.500     .
 1.650     ..
 1.800     .
 1.950     .
 2.100     .
 2.250     .
 2.400     *
 2.550     .
 2.700     .
 2.850     .
 3.000     *
 3.150     .
 3.300     .
 3.450     .
 3.600     .
 3.750     .
 3.900     .
 4.050     .*
 4.200     *
 4.350     *
 4.500     *
 4.650     *
 4.800     *
 4.950     .
 5.100     .
 5.250     .
 5.400     .
 5.550     .
 5.700     .
 5.850     .
 6.000     *
 6.150     *
 6.300     .
 6.450     .
 6.600     *
 6.750     *
 6.900     *
 7.050     *
 7.200     *
 7.350     *
 7.500     *
 7.650     *
```
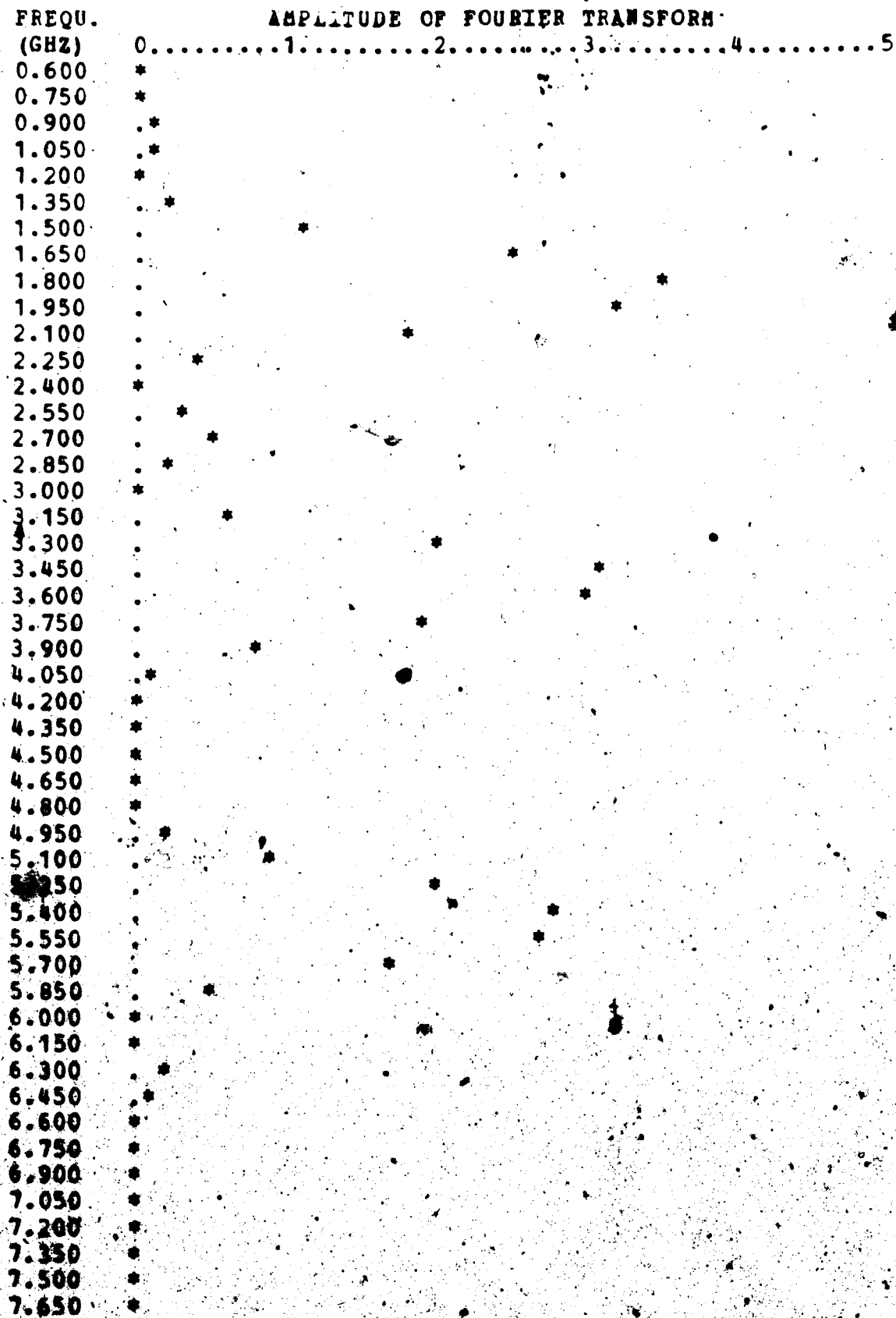
FIG. 12.   FOURIER TRANSFORM OF SYNTHETIC DATA I
           (FREQS IN GHZ: 1.6, 5.6, 5.4; AMP 1% NO FUSS)

FREQU.   AMPLITUDE OF FOURIER TRANSFORM
(GHZ)   0.........1.........2.........3.........4.........5

```
0.600
0.750
0.900
1.050
1.200
1.350
1.500
1.650
1.800
1.950
2.100
2.250
2.400
2.550
2.700
2.850
3.000
3.150
3.300
3.450
3.600
3.750
3.900
4.050
4.200
4.350
4.500
4.650
4.800
4.950
5.100
5.250
5.400
5.550
5.700
5.850
6.000
6.150
6.300
6.450
6.600
6.750
6.900
7.050
7.200
7.350
7.500
7.650
```

FIG.13. FOURIER TRANSFORM OF SYNTHETIC DATA II
(FREQS IN GHZ 1.0,3.0,5.0; AMPLES EQUAL)

```
FREQU.              AMPLITUDE OF FOURIER TRANSFORM
 (GHZ)      0.............1.........2.........3.........4.........5
 0.600      .   *
 0.750      . *
 0.900      . *
 1.050      . *
 1.200      . *
 1.350      .    *
 1.500      .       *
 1.650      t         *
 1.800      .       *
 1.950      .     *
 2.100      . *
 2.250      .   *
 2.400      .     *
 2.550      .     *
 2.700      .  *
 2.850      . *
 3.000      .    *
 3.150      .        *
 3.300      .          *
 3.450      .           *
 3.600      .        *
 3.750      .       *
 3.900      .      *
 4.050      .     *
 4.200      .    *
 4.350      .   *
 4.500      .  *
 4.650      .    *
 4.800      .   *
 4.950      .   *
 5.100      .    *
 5.250      .    *
 5.400      .     *
 5.550      .   *
 5.700      .  *
 5.850      . *
 6.000      .   *
 6.150      . *
 6.300      .  *
 6.450      .  *
 6.600      . *
 6.750      . *
 6.900      . *
 7.050      . *
 7.200      . *
 7.350      .
 7.500      .
 7.650      .
```
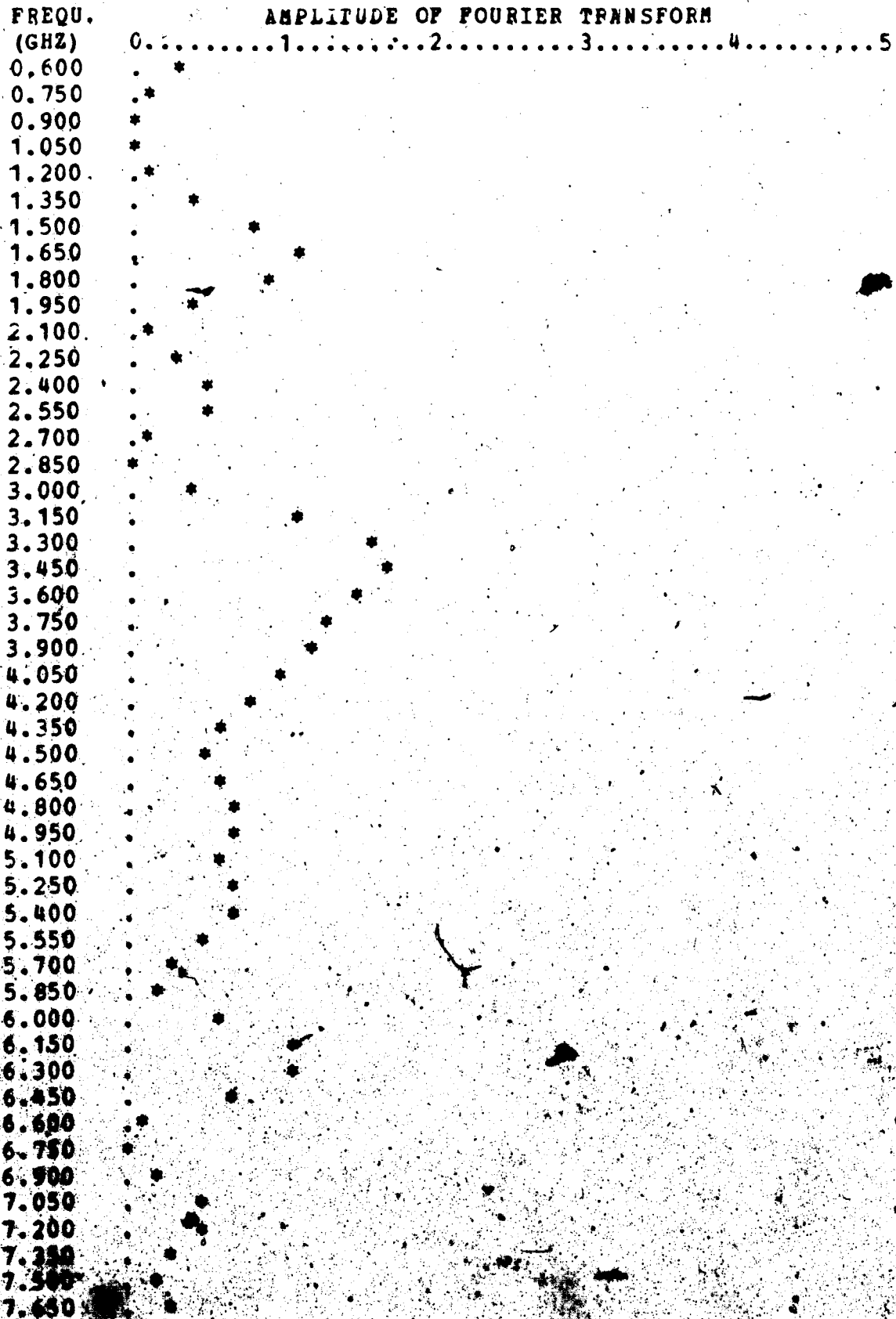
FIG.14. FOURIER TRANSFORM OF SYNTHETIC BAND III

actual boron data with 2% statistics. The first has a 1% beat amplitude with no scatter. The second and third have artificial scatter with beat amplitudes of 2% and 1% respectively. The 2% case has been strongly effected by FUZZ but the three frequencies are clearly larger than the noise. For the 1% case the "true" frequencies cannot be distinguished from the background.

Fig. 15 is a graph of theoretically possible frequencies calculated with the Stark-effect program mentioned in Chapter II. Three curves converge at zero field to the P-D Lamb shift at 1.42 GHz. Five converge to the D-F Lamb shift. No theoretical frequency is higher than the upper curve and lower than 51 GHz, the value of the S-P Lamb shift at zero field. It was hoped that Stark beats could be observed that would follow one or more of the upper curves to the P-D Lamb shift. In fact, no beat was observed with an amplitude greater than the statistics value of the data sample. In all, 33 beats were observed with amplitudes between 1% and 2.4%, and all fall randomly between 3 and 13.5 GHz. The conclusion is that these beats are noise and Stark beats in Boron V were not observed.

5.3 "Kck Beats"

In addition to the three data sets of hydrogen taken for field calibration, a fourth set of data
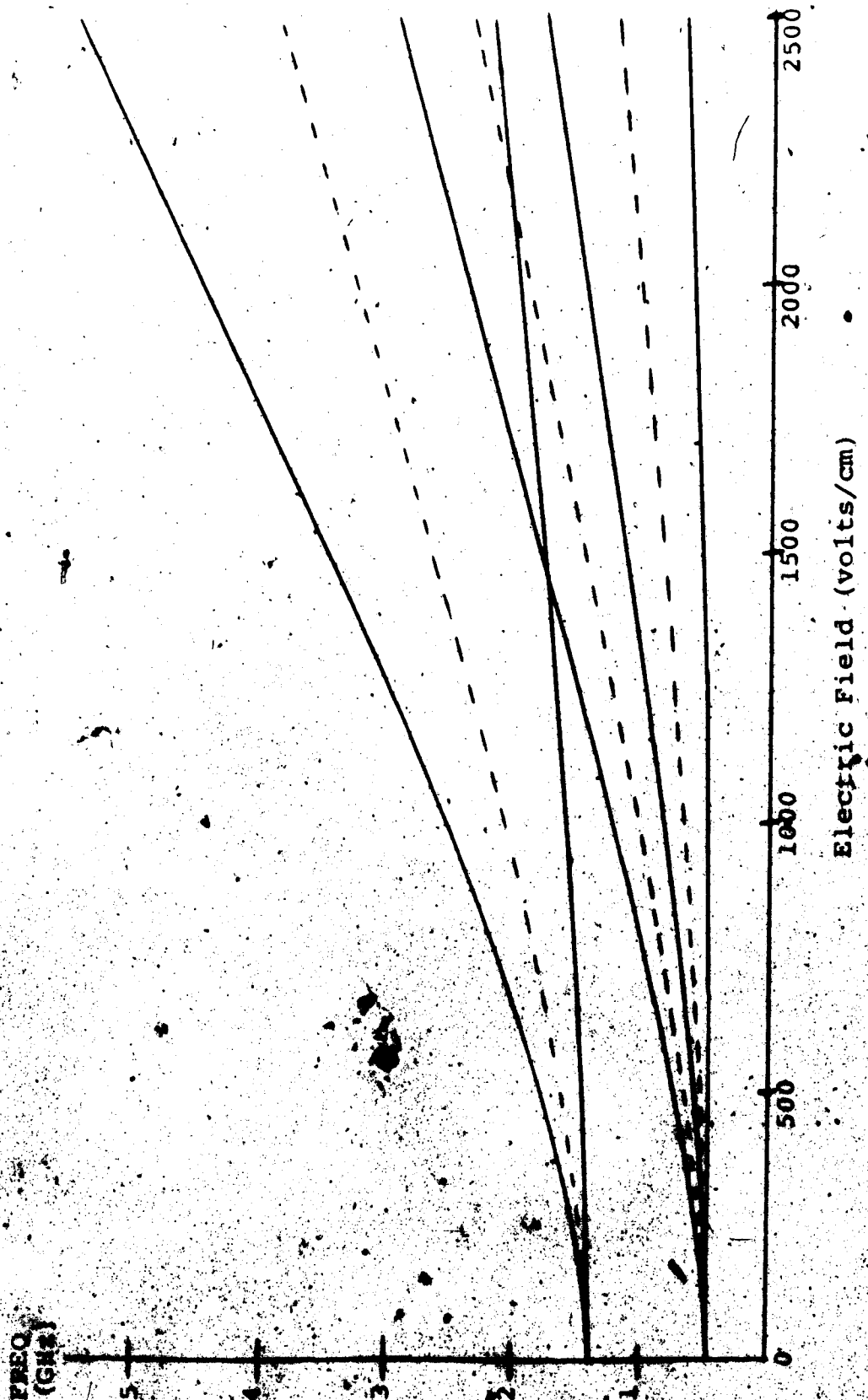
Fig. 15 Theoretical Beat Frequencies for Boron V (--- indicates forbidden at zero field)

was taken at +1,000 volts. The minus and plus 1 KV

data allow the relative cross section for S-P

coherence, σ_{sp}, to be evaluated, as in section 2.6.

The calculation will be outlined and the results

presented more as an indication of current quantum

beat research rather than the validity of the results.

The beat amplitudes were corrected for finite

beam acceptance length and the beats were added and

subtracted yielding:

$$I_+ + I_- = .100 \cos(\omega t - 80°) \tag{5.1}$$

$$I_+ - I_- = .056 \cos(\omega t + 36°) \tag{5.2}$$

To proceed with the calculation the values of σ_s, σ_{p_0}

and σ_{p_1} are required and these were taken from GAM.74.

Since only the relative values are known, the sum

$\sigma_s + \sigma_{p_0} + 2\sigma_{p_1}$ has been normalized. $\sigma_s = 0.5$,

$\sigma_{p_0} = 0.14$ and $\sigma_{p_1} = 0.15$. If equation (5.1) is

compared to (2:11), the modulation can be made a

negative cosine by adding -100° to the phase of (5.1).

This is equivalent to shifting the first point of the

sum back to the foil position. The constant term, V,

may then be calculated. Adding the same phase factor

to (5.2) and using Eq. (2.12) may be used to evaluate

σ_{sp}.

Table 5 lists the results for this experiment
at 333 KeV and those of Gaupp et al. (GAM 74) at the
other beam energies. The discrepancy motivated a
repeat of this part of the experiment by the group at
Argonne National Laboratory without the author's par-
ticipation. Attention was focused on duplicating the
starting point of the foil by taking plus and minus
data samples alternately and on obtaining better
statistics. The analysis of this new data is not yet
complete.

Table 5

Cross Section for S-P Coherence

H^+ Energy	Re σ_{sp}	Im σ_{sp}	$|\sigma_{sp}|$
110 KeV	-0.03	0.06	0.07
160 "	-0.09	0.17	0.19
210 "	-0.10	0.19	0.22
333 "	+0.14	0.12	0.19

5.4 Conclusion

To observe quantum beats many necessary condi-
tions must be satisfied. Chapter II discussed
coherence and alignment. The former is guaranteed
by the thin foil but the latter, while known to be

a property of foil excitation, is not guaranteed to be of sufficient magnitude to produce observable beats for any sample. Furthermore the mechanism for alignment is not yet understood so it is not possible to forecast the degree of alignment theoretically. Good spatial resolution is an obvious requirement for observation of high frequencies. When experiments are performed with equipment pushed to its design limit, as was the case with hydrogenic B V line in this project, it is easy not to satisfy the requirement and be unaware of this until after the experiment has been completed. The requirement for good statistics cannot be overemphasized. Often the spectral line of theoretical interest is not very intense and a compromise struck in the laboratory proves inadequate on the computer. The effect of cascades must also be considered. Whether or not alignment can be transferred by a cascade has yet to be definitely established. It seems best to choose a cascade-free transition if at all possible.

It is too early to conclude that the 2066 Å measurement was unsuccessful. Hyperfine beats are noted for their small amplitudes so further analysis is desirable. There are no quantum beats on our boron V data. To be properly performed the experiment

requires better spatial resolution and good statistics, which might be obtained if the 4 to 2 or 4 to 1 transition is observed with a grazing incidence spectrometer, which we do not have. The hydrogen quantum beats were clearly observed and the "Eck beat" calculation which has been presented is both current and controversial.

This work has been an attempt to review the entire field of quantum beat research and to present a description of early experiments and analysis performed at the University of Alberta. It is hoped that future work here will benefit from this endeavor.

BIBLIOGRAPHY

AD 73   M.J. Alguard and C.W. Drake, Phys. Rev. A 8, 27 (1973).

Al 63   E.B. Aleksandrov, Opt. & Spectrosc. (USA) 14, 232 (1963).

An 70   H.J. Andrä, Phys. Rev. Lett. 25, 325 (1970).

An 74   H.J. Andrä, Phys. Scr. 9, 257 (1974).

Ba 64   S. Bashkin, Nucl. Instr. Methods 28, 88 (1964).

Ba 68   Beam-Foil Spectroscopy, ed. S. Bashkin (Gordon and Breach, New York, 1968).

Ba 73   Proc. Third Int. Conf. Beam-Foil Spectroscopy, ed. S. Bashkin (North-Holland, Amsterdam, 1973); Nucl. Instr. Methods, 110, 1-522 (1973).

BBFW 65   S. Bashkin, W.S. Bickel, D. Fink and R.K. Wangsness, Phys. Rev. Lett. 15, 284 (1965).

BCES 74   H.G. Berry, L.J. Curtis, D.G. Ellis and R.M. Schectman, Phys. Rev. Lett. 32, 751 (1974).

Be 69   Data Reduction and Error Analysis for the Physical Sciences, Philip R. Bevington (McGraw-Hill Book Company, New York, 1969).

BG 74   J. Bosse and H. Gabriel, Z. Physik 266, 283 (1974).

BH 71   D.J. Burns and W.H. Hancock, Phys. Rev. Lett. 27, 370 (1971).

BH 73   D.J. Burns and W.H. Hancock, J. Opt. Soc. Am. 63, 241 (1973).

BPS 74   H.G. Berry, E.H. Pinnington, J.L. Subtil, Phys. Rev. A 10, 1065 (1974).

Br 33   G. Breit, Rev. Mod. Phys. 5, 91 (1933).

BSC 72   H.G. Berry, J.L. Subtil a[...]ré, Journal de Physique 33, 947 (197[...).

BSPAWG 73 H.G. Berry, J.L. Subtil, E.H. Pinnington, H.J. Andrä, W. Wittman and A. Gaupp, Phys. Rev. A 7, 1609 (1973).

CL 73   D.A. Church and C.H. Liu, Physica 67, 90
           (1973).

CP 66   Thomas R. Carver and Robert B. Partridge, Am.
           J. Phys. 34, 339 (1966).

CS 63   The Theory of Atomic Spectra, E.U. Condon and
           G.H. Shortley (Cambridge Univ. Press, London,
           1963).

DAWB 72   P. Dobberstein, H.J. Andrä, W. Wittman and
           H.H. Bukow, Z. Physik 257, 272 (1972).

Ec 73   T.G. Eck, Phys. Rev. Lett. 31, 270 (1973).

Ed 57   Angular Momentum in Quantum Mechanics,
           A.R. Edmonds (Princeton Univ. Press, Princeton,
           N.J., 1957).

El 73   David G. Ellis, J. Opt. Soc. Am. 63, 1232
           (1973).

EY 65   G.W. Erickson and D.R. Yennie, Ann. Phys.(USA)
           35, 271 (1965).

Fa 57   U. Fano, Rev. Mod. Phys. 29, 74 (1957).

FM 73   U. Fano and Joseph H. Macek, Rev. Mod. Phys.
           45, 553 (1973).

GAM 74   A. Gaupp, H.J. Andrä and J. Macek, Phys. Rev.
           Lett. 32, 268 (1974).

GCBL 73   M. Gaillard, M. Carré, H.G. Berry and M.
           Lombardi, Nuclear Instr. Methods 110, 273
           (1973).

GM 65   J.D. Garcia and J.E. Mack, J. Opt. Soc. Am.
           55, 654 (1965).

GS 66   W.M. Gentleman and G. Sande, AFIPS 29, 563,
           Fall Joint Computer Conference (1966).

Ha 56   John M. Harriman, Phys. Rev. 101, 594 (1956).

IL 74   D.J.G. Irwin and A.E. Livingston, Computer
           Physics Communications 7, 95 (1974).

IL 75   D.J.G. Irwin and A.E. Livingston, to be
           published.

La 52   W. Lamb, Phys. Rev. <u>85</u>, 259 (1952).

LBC 74   C.H. Liu, S. Bashkin and D.A. Church, Phys.
          Rev. Lett. <u>33</u>, 993 (1974).

LGM 75   Maurice Lombardi, Marc Giroud and Joseph Macek,
          Phys. Rev. A <u>11</u>, 1114 (1975).

Li 71   C.C. Lin, University of Alberta thesis
          (unpublished).

Li 74   A.E. Livingston, University of Alberta thesis
          (unpublished).

Lo 73   The Quantum Theory of Light, Rodney Loudon
          (Oxford Univ. Press, London, 1973).

Lü 51   G. Lüders, Ann. Physik <u>6</u>, 301 (1951).

Ma 69   J. Macek, Phys. Rev. Lett. <u>23</u>, 1 (1969).

Ma 70   Joseph Macek, Phys. Rev. A <u>1</u>, 618 (1970).

MBB 70   Proc. Second Int. Conf. Beam-Foil Spectroscopy,
          ed. I. Martinson, J. Bromander and H.G. Berry
          (North-Holland, Amsterdam, 1970); Nucl. Instr.
          Methods <u>90</u>, 1-371 (1970).

MG 74   I. Martinson and A. Gaupp, Physics Reports
          (Section C of Physics Letters) <u>15</u>, 113 (1974).

Mi 70   Quantum Mechanics of Atomic Spectra and Atomic
          Structure, Masataka Mizushima (W.A. Benjamin,
          Inc., New York, 1970).

NS 70   L.C. Northcliffe and R.F. Schilling, Nuclear
          Data Tables, <u>A7</u>, 233 (1970).

PBDS 73   E.H. Pinnington, H.G. Berry, J. Désesquelles
          and J.L. Subtil, Nucl. Instr. Methods <u>110</u>,
          315 (1973).

WTAD 72   W. Wittman, K. Tillmann, H.J. Andrä and P.
          Dobberstein, Z. Physik <u>257</u>, 279 (1972).

THE PROGRAMS

```
C        FOURIER TRANSFORM USING HOMER FIT
C

         DIMENSION OSCN(400),BEAT(400),BKGD(400),LINE(71)
         INTEGER DOT,STAR,BLANK,SIG(400)
         INTEGER WORDS(72)
         DATA DOT/1H./,STAR/1H*/,BLANK/1H /
   50    READ(5,201) N,MIN,MAX,SCALE,STEP,FINCR,SIZE,ENLO
         IF(N.LT.1) GO TO 60
         READ(5,205) WORDS
         READ(4,202) (SIG(I),I=1,N)
         READ(3,210) TA,A0,A2,TB,A4,TC,VEL
         WRITE(6,100) WORDS
         WRITE(6,109)SCALE
C
C        EVALUATE BACKGROUND PARAMETERS
C        USING HOMER FIT
C
         IF(TA) 16,16,17
   16    A1=0.
         GOTO 20
   17    A1=-STEP/(VEL*TA)
         IF(TB) 20,20,25
   20    A3=0.
         GOTO 30
   25    A3=-STEP/(VEL*TB)
         IF(TC) 30,30,35
   30    A5=0.
         GOTO 40
   35    A5=-STEP/(VEL*TC)
C
C        CALCULATE BEAT AMPLITUDE
C
   40    BTSUM=0.0
         DO 6 I=1,N
         QI=(I-1)
         BKGD(I)=A0*EXP(A1*QI)+A2*EXP(A3*QI)
        *+A4*EXP(A5*QI)
         OSCN(I)=SIG(I)-BKGD(I)
         IF(BKGD(I)) 5,5,7
   5     BEAT(I)=OSCN(I)
         GOTO 6
   7     BEAT(I)=OSCN(I)/BKGD(I)
   6     BTSUM=BTSUM+BEAT(I)*BEAT(I)
         APRX=8.0*BTSUM*N/9.8696
         WRITE(6,110) APRX
         WRITE(6,104)
         WRITE(6,102) (SIG(I),BKGD(I),OSCN(I),BEAT(I),I=1,N)
C
C        CALCULATE FOURIER TRANSFORM
C
```

```
      WRITE(6,101)
      DO 15 I=1,71
15    LINE(I)=BLANK
      DO 10 I=MIN,MAX
      LINE( 1)=DOT
      QS=I-1
      EN=ENLO+FINCR*QS
      SUMSIN=0.0
      SUMCOS=0.0
      P=EN*SCALE
      DO 11 J=1,N
      QT=J-1
      ARG=2.*3.14159*P*QT
      SUMSIN=SUMSIN+BEAT(J)*SIN(ARG)
      SUMCOS=SUMCOS+BEAT(J)*COS(ARG)
11    CONTINUE
      SUMSQD=SUMSIN*SUMSIN+SUMCOS*SUMCOS
      FREQ=EN*30.0
C
C         PLOT FOURIER TRANSFORM
C
C
      IY=1.+SUMSQD*SIZE/APRX
      LINE(IY)=STAR
      WRITE(6,107)SUMSQD,SUMSIN,SUMCOS,FREQ,EN,LINE
      LINE(IY)=BLANK
10    CONTINUE
      GO TO 50
60    WRITE(6,108)
      STOP
100   FORMAT(1H1,72A1)
101   FORMAT('1',4X,'SUMSQD',6X,'SUMSIN',6X,'SUMCOS',4X,
     *'FREQU.',2X,'ENERGY',30X,'AMPLITUDE OF FOURIER',
     *' TRANSFORM',/39X,' (GHZ) ',3X,'(CM-1)',
     *7X,'0.........1.........2.........3.........',
     *'4.........5.........6.........7')
102   FORMAT(I10,5X,3E15.6)
104   FORMAT(1H0,4X,'SIG(I)',8X,'BKGD(I)',8X,'OSCN(I)'
     *,8X,'BEAT(I)')
107   FORMAT(1H ,3E12.4,2F8.4,7X,71A1)
108   FORMAT(1H1,50X,'THE END')
109   FORMAT(1H-,14HSCALE FACTOR =,F6.3,
     *21H/(CHANNEL*WAVENUMBER))
110   FORMAT(1H0,'MAX SUMSQD = ',E10.4)
201   FORMAT(3I3,1X,5F10.5)
202   FORMAT(/,/,(5(3X,I6,5X)))
205   FORMAT(72A1)
210   FORMAT(/,19X,F9.4,2F11.2,F10.4,F10.2,F10.4,/,/,
     *73X,F5.3)
      END
```

```
C      BEAT AMPLITUDE EVALUATION WITH PLOT
C
C
       INTEGER SIG(256),WORDS(72),DOT,STAR,BLANK,AMPL(256)
      *,FLGPLT
       DIMENSION LINE(100),FREQ(256),BKGD(256)
       DATA DOT/1H./,STAR/1H*/,BLANK/1H /
       PI=3.14159
   15  READ(5,130) WORDS
       READ(5,120) N,MAX,SCALE,STEP,FINCR,FREQ1,FLGPLT
       IF(N.EQ.0) STOP
       WRITE(6,200) WORDS
       WRITE(6,202) SCALE
       READ(3,100) IDF,NHP
       READ(3,105) TA,A0,A2,TB,A4,TC,VEL
       READ(4,110) (SIG(I),I=1,N)
       A1=-STEP/(VEL*TA)
        IF(TB) 20,20,25
   20  A3=0.
       GOTO 30
   25  A3=-STEP/(VEL*TB)
       IF(TC) 30,30,35
   30  A5=0.
       GOTO 40
   35  A5=-STEP/(VEL*TC)
C
C
C      EVALUATE BKGD, STATS AND CHISQO
C
   40  CHISQO=0.
       STSUM=0.
       DO 45 I=1,N
       BKGD(I)=A0*EXP(A1*(I-1))+A2*EXP(A3*(I-1))+
      *A4*EXP(A5*(I-1))
       STSUM=STSUM+SQRT(FLOAT(SIG(I)))/SIG(I)
   45  CHISQO=CHISQO+((SIG(I)-BKGD(I))**2)/SIG(I)
       STATS=100*STSUM/N
       NFP=NHP-IDF
       RFP=FLOAT(N)/NHP*NFP
       CHISQO=CHISQO/(N-RFP)
       WRITE(6,205) CHISQO,STATS
       WRITE(6,210)
       WRITE(6,220)
       DO 70 L=1,MAX
       FREQ(L)=FREQ1+(L-1)*FINCR
       Y1=2*PI*FREQ(L)*SCALE/29.979
C
C
C    2 PARAMETER LINEAR LEAST SQUARES FIT
C     TO AMPLITUDE AND PHASE
C
       B11=0.
       B12=0.
       B22=0.
       R1=0.
```

```
      R2=0.
      CHISQ=0.
C
C     ENTER SUMMATION LOOP
C
      DO 50 I=1,N
      B1=COS(Y1*(I-1))*BKGD(I)
      B2=SIN(Y1*(I-1))*BKGD(I)
      B11=B11+B1*B1/SIG(I)
      B12=B12+B1*B2/SIG(I)
      B22=B22+B2*B2/SIG(I)
      R1=R1+B1-BKGD(I)*B1/SIG(I)
      R2=R2+B2-BKGD(I)*B2/SIG(I)
50    CONTINUE
C
C     EVALUATE AMPLITUDES AND UNCERTAINTIES.
C
      DET=B11*B22-B12*B12
      AMP1=(R1*B22-R2*B12)/DET
      AMP2=(B11*R2-R1*B12)/DET
      UAMP1=B22/DET
      UAMP2=B11/DET
      UAMP12=-2*B12/DET
C
C     CHANGE VARIABLES TO COSINE
C     AMPLITUDE AND PHASE
C
      AMP12=AMP1*AMP1
      AMP22=AMP2*AMP2
      AMP=SQRT(AMP12+AMP22)
      PHS=ATAN2(AMP2,AMP1)
      UAMP=(UAMP1*AMP12+UAMP2*AMP22
     *+UAMP12*AMP1*AMP2)/(AMP12+AMP22)
      UPHS=(UAMP1*AMP22+UAMP2*AMP12-UAMP12
     *+AMP1*AMP2)/(AMP12+AMP22)**2
      UAMP=SQRT(UAMP)*100.
      UPHS=SQRT(UPHS)*360./(2*PI)
C
C     EVALUATE CHISQ
C
      DO 60 I=1,N
      PCTN=BKGD(I)*(1+AMP1*COS(Y1*(I-1))+AMP2*
     *SIN(Y1*(I-1)))
60    CHISQ=CHISQ+((SIG(I)-PCTN)**2)/SIG(I)
      AMPP=AMP*100.
      PHS=PHS*360./(2*PI)
      CHISQR=CHISQ/(N-REP-2)
      AMPL(L)=ABS(1000*AMP)
      WRITE(6,230) FREQ(L),AMPP,UAMP,PHS,UPHS,CHISQ,CHISQR
70    CONTINUE
C
C     PLOT RESULTS
C
      IF(FLGPLT.EQ.0) GOTO 15
```

```
      DO 80 I=1,100
   80 LINE(I)=BLANK
      WRITE(6,250)
      WRITE(6,260)
      DO 90 I=1,MAX
      LINE(1)=DOT
      LINE(1+AMPL(I))=STAR
      WRITE(6,270) FREQ(I),LINE
   90 LINE(1+AMPL(I))=BLANK
      GOTO 15
  100 FORMAT(33X,I3,31X,I3)
  105 FORMAT(19X,F9.4,2F11.2,F10.4,F10.2,F10.4,
     */,/,73X,F5.3)
  110 FORMAT(/,/,(5(3X,I6,5X)))
  120 FORMAT(2I3,4F10.5,I1)
  130 FORMAT(72A1)
  200 FORMAT(1H1,6X,72A1)
  202 FORMAT(1H0,6X,14HSCALE FACTOR =,F6.3,
     *21H/(CHANNEL*WAVENUMBER))
  205 FORMAT(1H0,6X,25HREDUCED CHISQD W/O BEAT =,F7.3,
     *15X,7HSTATS =,F4.1,1HX)
  210 FORMAT(1H0,10X,9HFREQUENCY,7X,9HAMPLITUDE,6X,
     *11HUNCERTAINTY,8X,5HPHASE,8X,11HUNCERTAINTY,
     *13X,11HCHI-SQUARED)
  220 FORMAT(13X,5H(GHZ),9X,9H(PERCENT),9X,5H(AMP),9X,
     *9H(DEGREES),9X,5H(PHS),25X,9H(REDUCED),/)
  230 FORMAT(1X,F17.3,F16.3,F16.3,F16.1,F16.2,F16.2,F16.3)
  250 FORMAT(1H1,6X,9HFREQUENCY,42X,
     *25HBEAT AMPLITUDE IN PERCENT)
  260 FORMAT(10X,3HGHZ,8X,20H0.........1........,
     *40H2.........3.........4.........5........,
     *42H6.........7.........8.........9........10)
  270 FORMAT(1X,F13.3,7X,100A1)
      END
```

```
C      FUZZ ROUTINE
       IMPLICIT LOGICAL (L), REAL*8 (D)
       INTEGER STEP (400)
C  THIS SUBROUTINE RANDOMIZES DATA IN FKS,
C  FKS BEING THE MEANS
       DATA GAUSSL /37.0/
C  FOLLOWING DEFINES VARIABLES FOR RANDOM NUMBER GENERATION
       DIMENSION ISTART(5) ,FKS(400),IFKS(400)
       DATA ISTART /718415745,1039450965,998356979,
      *124005191,1035698051/
       DATA MULT /32771/
       DATA ISIZE /1073741824/
       DATA DNORM /2147483648.D0/
     1 READ(5,200) M1,N
       READ(5,205) VEL,A,TA,B,TB,C,TC,M2
       READ(5,215) (STEP(I),FKS(I),I=1,N)
C
       READ(4,230) KSET
       IRAND=ISTART(KSET+1)
C
       DO 50 IKS=1,N
C  COMPUTE RANDOM NUMBER BETWEEN -.5 AND +.5
       IRAND=MOD(IRAND*MULT,ISIZE)
       DRAND=DFLOAT(IRAND)/DNORM
       PN=FKS(IKS)
C  IF MEAN IS ZERO NO VALUE OTHER THAN ZERO IS POSSIBLE
       IF(PN.LE.0.0D0) GO TO 50
C  IF THE MEAN, PN, IS GREATER THAN GAUSSL
C  IT IS CONSIDERED GAUSSIAN
       IF(PN.GT.GAUSSL) GO TO 40
C  USE TRUE POISSON DISTRIBUTION BY CUMULATIVE SUMS
       DN=DBLE(PN)
       IF(DRAND.LT.0.0D0) DRAND=DRAND+1.0D0
       DP=DEXP(-DN)
       DSUM=DP
C  THE COUNT USED IS THE INDEX WHEN THE SUM EXCEEDS RAND
       DO 20 I=1,100
       IF(DSUM.LT.DRAND) GO TO 15
       FKS(IKS)=FLOAT(I-1)
       GO TO 50
    15 DP=DP*DN/DFLOAT(I)
       DSUM=DSUM+DP
    20 CONTINUE
       WRITE(6,100)
   100 FORMAT(' FUZZ - UPPER LIMIT EXCEEDED')
       GO TO 50
C  MEAN IS TOO LARGE TO USE POISSON. GAUSSIAN IS ASSUMED
C  FORMULA OBTAINED FROM:
C  APPROXIMATIONS FOR DIGITAL COMPUTERS, CECIL HASTINGS JR.
C  PRINCETON UNIVERSITY PRESS, PRINCETON, NEW JERSEY, U.S.A.
    40 RAND=SNGL(DRAND)
       ETA=SQRT(-ALOG(RAND**2))
```

```
      X=(.010328*ETA+.802853)*ETA+2.515517
      X=X/(((.001308*ETA+.189269)*ETA+1.432788)*ETA+1.0)
      X=-SIGN(ETA-X,RAND)
      FKS(IKS)=FN+X*SQRT(FN)
      IFKS(IKS)=IFIX(FKS(IKS))
   50 CONTINUE
      WRITE(6,200) M1,N
      WRITE(6,210) VEL,A,TA,B,TB,C,TC,M2
      WRITE(6,220) (STEP(I),IFKS(I),I=1,N)
      KSET=KSET+1
      IF(KSET.EQ.5) KSET=0
      WRITE(4,230) KSET
      IF(N.GT.1) GOTO 1
      STOP
  200 FORMAT(16X,I2,52X,I2)
  205 FORMAT(23X,F5.3,1X,F5.0,1X,F7.3,1X,F5.0,1X,F7.3,
     *1X,F5.0,1X,F7.3,1X,I1)
  210 FORMAT(23X,F5.3,1X,F6.0,F8.3,F6.0,F8.3,F6.0,F8.3,I1)
  215 FORMAT((5(I3,F6.0,5X)))
  220 FORMAT((5(I3,I6,5X)))
  230 FORMAT(I2)
      END
```